AD-A162 589 INVESTIGATION OF STEELS FOR IMPROVED WELDABILITY IN SHIP CONSTRUCTION(U) UNITED STATES STEEL CORP MONROEVILLE PA L J CUDDY ET AL. MAY 84 SR-1256-3 1/1

UNCLASSIFIED DOT-CG-80588-A F/G 11/6 NL

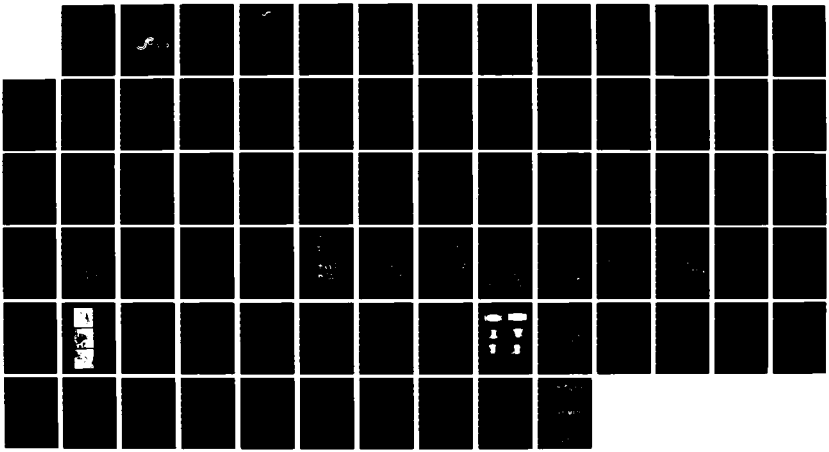

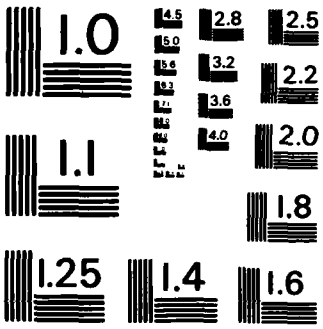

MICROCOPY RESOLUTION TEST CHART
NATIONAL BUREAU OF STANDARDS-1963-A

SSC-327

INVESTIGATION OF STEELS FOR IMPROVED WELDABILITY IN SHIP CONSTRUCTION PHASE III

AD-A162 589

DTIC
ELECTE
DEC 13 1985
S D
D

This document has been approved for public release and sale; its distribution is unlimited

DTIC FILE COPY

SHIP STRUCTURE COMMITTEE
1985

85 12 13 029

SHIP STRUCTURE COMMITTEE

THE SHIP STRUCTURE COMMITTEE is constituted to prosecute a research program to improve the hull structures of ships and other marine structures by an extension of knowledge pertaining to design, materials and methods of construction.

RADM C. T. Lusk, Jr., USCG (Chairman)
Chief, Office of Merchant Marine Safety
U. S. Coast Guard Headquarters

Mr. T. W. Pross
Associate Administrator for Shipbuilding, Operations & Research
Maritime Administration

Mr. P. M. Palermo
Executive Director
Ship Design & Integration Directorate
Naval Sea Systems Command

Mr. J. B. Gregory
Chief, Technology Assessment & Research Branch
Minerals Management Service

Mr. W. M. Hannan
Vice President
American Bureau of Shipping

Mr. T. W. Allen
Engineering Officer
Military Sealift Command

CDR D. B. Anderson, U. S. Coast Guard (Secretary)

SHIP STRUCTURE SUBCOMMITTEE

The SHIP STRUCTURE SUBCOMMITTEE acts for the Ship Structure Committee on technical matters by providing technical coordination for the determination of goals and objectives of the program, and by evaluating and interpreting the results in terms of structural design, construction and operation.

U. S. COAST GUARD

CAPT A. E. HENN
CAPT J. R. WALLACE
MR. J. S. SPENCER
MR. R. E. WILLIAMS

NAVAL SEA SYSTEMS COMMAND

MR. J. B. O'BRIEN (CHAIRMAN)
CDR R. BUBECK
MR. J. E. GAGORIK
MR. A. B. ENGLE
MR. S. G. ARNTSON (COTR)
MR. G. WOODS (COTR)

MARITIME ADMINISTRATION

MR. F. SEIBOLD
MR. N. O. HAMMER
DR. W. M. MACLEAN
MR. M. W. TOUMA

NATIONAL ACADEMY OF SCIENCES
COMMITTEE ON MARINE STRUCTURES

MR. A. DUDLEY HAFF - LIAISON
MR. R. W. RUMKE - LIAISON

SOCIETY OF NAVAL ARCHITECTS & MARINE ENGINEERS

MR. N. O. HAMMER - LIAISON
MR. F. SELLARS - LIAISON

WELDING RESEARCH COUNCIL

DR. G. W. OYLER - LIAISON

MILITARY SEALIFT COMMAND

MR. D. STEIN
MR. T. W. CHAPMAN
MR. A. ATTERMEYER
MR. A. B. STAVOVY

AMERICAN BUREAU OF SHIPPING

DR. D. LIU
MR. I. L. STERN
MR. B. NADALIN

MINERALS MANAGEMENT SERVICE

MR. R. GIANGERELLI
MR. R. C. E. SMITH

INTERNATIONAL SHIP STRUCTURES CONGRESS

MR. S. G. STIANSEN - LIAISON

AMERICAN IRON & STEEL INSTITUTE

MR. J. J. SCHMIDT - LIAISON

STATE UNIVERSITY OF NY MARITIME COLLEGE

DR. W. R. PORTER - LIAISON

U.S. COAST GUARD ACADEMY

LT J. TUTTLE - LIAISON

U.S. NAVAL ACADEMY

DR. R. BHATTACHARYYA - LIAISON

U.S. MERCHANT MARINE ACADEMY

DR. C. B. KIM - LIAISON

Member Agencies:

United States Coast Guard
Naval Sea Systems Command
Maritime Administration
American Bureau of Shipping
Military Sealift Command
Minerals Management Service

Ship Structure Committee

An Interagency Advisory Committee
Dedicated to the Improvement of Marine Structures

Address Correspondence to:

Secretary, Ship Structure Committee
U.S. Coast Guard Headquarters, (G-M/TP 13)
Washington, D.C. 20593
(202) 426-2197

SR-1256

Much of the modernization taking place in the world shipbuilding industry in the last decade has centered around the use of new, more efficient welding techniques. The potential increase in productivity with new high-deposition rate welding processes is considerable. However, in order to take full advantage of the benefits of the new welding practices, additional metallurgical control appears necessary for minimizing heat-affected zone and weld-metal property degradation.

The Ship Structure Committee (SSC) sponsored a project directed toward determining the weld procedure and metallurgical control necessary to develop adequate toughness in the weldment, using high-deposition rate welding procedures. Two previous reports (SSC-298 and SSC-305) detailed the first two phases of this effort. This volume describes the third and final phase, giving the overall conclusions and recommendations.

CLYDE T. LUSK, Jr.
Rear Admiral, U.S. Coast Guard
Chairman, Ship Structure Committee

Technical Report Documentation Page

1. Report No. SSC-327	2. Government Accession No. AD-A162 589	3. Recipient's Catalog No.
4. Title and Subtitle Investigation of Steels for Improved Weldability in Ship Construction		5. Report Date May 1984
		6. Performing Organization Code
7. Author(s) L. J. Cuddy, J.S. Lally, and L.F. Porter		8. Performing Organization Report No. SR-1256
9. Performing Organization Name and Address U. S. Steel Corporation Technology Center One Tech Center Drive Monroeville, PA 15146		10. Work Unit No. (TRAIS)
		11. Contract or Grant No. DOT-CG-80588-A
12. Sponsoring Agency Name and Address U. S. Coast Guard Office of Merchant Marine Safety Washington, D. C. 20593		13. Type of Report and Period Covered Final Report
		14. Sponsoring Agency Code G-M

15. Supplementary Notes

16. Abstract

This is the third and final phase of a multi-year effort aimed at investigating those factors which influence the microstructure in the Heat Affected Zone (HAZ) of economically produced ship plates with high yeild strengths when subjected to high heat inputs such as electroslag and submerged arc welding. The Ship Structure Committee has published the first two phases as SSC-298 and SSC-305.

17. Key Words Weld, Heat Affected Zone, Steel, Toughness, Rare-Earth Metals, Submerged Arc Weld, Electroslag Weld, Charpy V-notch	18. Distribution Statement This document is available through the National Technical Information Service Springfield, VA 22161

19. Security Classif. (of this report)	20. Security Classif. (of this page)	21. No. of Pages	22. Price
Unclassified	Unclassified	72	

Form DOT F 1700.7 (8-72) Reproduction of completed page authorized

METRIC CONVERSION FACTORS

Approximate Conversions to Metric Measures

Symbol	When You Know	Multiply by	To Find	Symbol
		LENGTH		
in	inches	*2.5	centimeters	cm
ft	feet	30	centimeters	cm
yd	yards	0.9	meters	m
mi	miles	1.6	kilometers	km
		AREA		
in^2	square inches	6.5	square centimeters	cm^2
ft^2	square feet	0.09	square meters	m^2
yd^2	square yards	0.8	square meters	m^2
mi^2	square miles	2.6	square kilometers	km^2
	acres	0.4	hectares	ha
		MASS (weight)		
oz	ounces	28	grams	g
lb	pounds	0.45	kilograms	kg
	short tons (2000 lb)	0.9	tonnes	t
		VOLUME		
tsp	teaspoons	5	milliliters	ml
Tbsp	tablespoons	15	milliliters	ml
fl oz	fluid ounces	30	milliliters	ml
c	cups	0.24	liters	l
pt	pints	0.47	liters	l
qt	quarts	0.95	liters	l
gal	gallons	3.8	liters	l
ft^3	cubic feet	0.03	cubic meters	m^3
yd^3	cubic yards	0.76	cubic meters	m^3
		TEMPERATURE (exact)		
°F	Fahrenheit temperature	5/9 (after subtracting 32)	Celsius temperature	°C

*1 in = 2.54 (exactly). For other exact conversions and more detailed tables, see NBS Misc. Publ. 286, Units of Weights and Measures, Price $2.25, SD Catalog No. C13.10:286.

Approximate Conversions from Metric Measures

Symbol	When You Know	Multiply by	To Find	Symbol
		LENGTH		
mm	millimeters	0.04	inches	in
cm	centimeters	0.4	inches	in
m	meters	3.3	feet	ft
m	meters	1.1	yards	yd
km	kilometers	0.6	miles	mi
		AREA		
cm^2	square centimeters	0.16	square inches	in^2
m^2	square meters	1.2	square yards	yd^2
km^2	square kilometers	0.4	square miles	mi^2
ha	hectares (10,000 m^2)	2.5	acres	
		MASS (weight)		
g	grams	0.035	ounces	oz
kg	kilograms	2.2	pounds	lb
t	tonnes (1000 kg)	1.1	short tons	
		VOLUME		
ml	milliliters	0.03	fluid ounces	fl oz
l	liters	2.1	pints	pt
l	liters	1.06	quarts	qt
l	liters	0.26	gallons	gal
m^3	cubic meters	35	cubic feet	ft^3
m^3	cubic meters	1.3	cubic yards	yd^3
		TEMPERATURE (exact)		
°C	Celsius temperature	9/5 (then add 32)	Fahrenheit temperature	°F

Abstract

Simulated high-heat-input welding cycles (up to 1000 kJ/inch) have been employed to develop a grain-coarsened heat-affected-zone (HAZ) microstructure in a series of steels. The effects of titanium, vanadium, residuals, and nitrogen additions on the microstructures and properties in the HAZ of aluminum-killed steel containing 0.12%C and 1.35%Mn were determined.

Two factors influenced HAZ toughness, the volume fraction of martensite and the level of free nitrogen, both of which are influenced by the presence of TiN particles. At high levels of Ti and N, the TiN particles pin grain boundaries and thereby lessen austenite grain coarsening. They also interact with ledges on Widmanstatten side plates to impede plate growth and increase the density of stabilized ledges that nucleate pearlite instead of martensite as the minor transformation product. In the absence of rapid Widmanstatten growth, ferrite is nucleated intragranularly to produce an equiaxed ferrite/pearlite morphology. Despite the desirable microstructure, HAZ toughness is poor because of the high level of nitrogen. At intermediate levels of Ti and N, grain boundary pinning is minimal, but the equiaxed ferrite/pearlite structure remains to produce good toughness. At low levels of Ti and N, the grain size and ferrite morphology resemble those of the base steel; but toughness is excellent, independent of microstructure, because of low free nitrogen.

Accesion For
NTIS CRA&I ☑
DTIC TAB ☐
Unannounced ☐
Justification
By
Distribution /
Availability Codes
Dist | Avail and / or Special
A-1

QUALITY INSPECTED 3

Contents

Page

Introduction.....1

Materials and Experimental Work.....2
- Materials.....2
- Gleeble Treatment.....3
- Welding.....3
- Microstructures and Fractography.....4

Results.....4
- Base-Plate Properties and Microstructures.....4
- Simulated HAZ's.....5
- Fracture-Path Studies.....9
- The Roles of N and TiN.....10
- Development of the Transformation Products.....12
- Weldments.....13

Discussion.....15

Conclusions.....18

Recommendations.....18

References.....20

List of Tables.....21

List of Figures.....36

APPENDIX A Temperature Measurements in Weld Heat-Affected Zones.....A-1

APPENDIX B Individual Transverse Charpy V-Notch Test Results from Base Plates.....B-1

APPENDIX C Individual Charpy V-Notch Test Results from the HAZ of Electroslag-Welding and Submerged-Arc-Welding Gleeble Simulations.....C-1

APPENDIX D Individual Charpy V-Notch Test Results from the HAZ of Electroslag and Submerged-Arc Welded Steels.....D-1

Introduction

The purpose of Phase III of this contract is to further develop ship plate steels following on the work done in Phase II. As the initial task of Phase III, the microstructures and properties produced in the heat affected zone (HAZ) of Phase II steels were re-evaluated. Data for five steels that are representative of the results of Phase II are shown in Table I. Some typical microstructures of these steels are shown in Figure 1.

Addition of titanium to the base steel improved the toughness of the HAZ by refining the austenite grain size and by changing transformation products from Widmanstatten ferrite, pearlite, and bainite to a more equiaxed ferrite and pearlite microstructure. Additions of residuals (Cu + Ni + Cr + Mo) to the base steel degraded the HAZ toughness, whereas the addition of titanium with the residuals restored the toughness to the values similar to those in the base steel. The addition of residuals produced Widmanstatten ferrite, whereas residuals plus titanium again produced a more equiaxed ferrite. A steel containing 0.08%V exhibited structure and properties similar to the base steel. It was not clear from these results just what microstructural feature(s) controlled the HAZ toughness.

Based on this assessment, 17 new heats were melted and processed into plate for testing of the HAZ properties and microstructures produced by weld simulation and by actual welding. Welding simulation was first used to evaluate the performance of 15 heats whose composition was predicated on work done in Phase II. Two heats, whose composition was based on the best results of the 15-heat simulation study, were then made so that real weldments could be evaluated. Particular attention was focused on trying to determine the relationship between the microstructures that evolved in the HAZ and the properties that developed. Additional studies to determine how the HAZ microstructure developed on cooling after welding were done by quenching specimen blanks in the cooling phase of a Gleeble

simulation in the temperature range 1292 to 662°F. Also a study was performed to determine if a relation could be observed between the fracture path in Charpy V-notch (CVN) test specimens and the microstructure produced in the HAZ. These results were used to explain how the improved properties observed in the HAZ of some steels in this project were affected by titanium nitride precipitates, total nitrogen content, and residual levels.

Materials and Experimental Work

Materials

Table II shows the chemical composition of 17 laboratory-melted steels used in Phase III of this project. Fifteen of the steels were 300-pound (136 kg) heats induction-melted in a vacuum furnace and poured into slab ingot molds. Two 500-pound (227 kg) heats were subsequently made of the best compositions in order to test actual weldments. All the ingots were air cooled to room temperature. The fifteen 300-pound ingots were reheated to 2350°F and rolled longitudinally to 1/2-inch-thick (12.7 mm) plate with a final-pass temperature of 1900°F (1040°C) as measured by an optical pyrometer. The two 500-pound ingots were rolled to 1-inch-thick (25.4 mm) plate using the same reheat finishing temperatures above. After rolling, the plates from all the steels were normalized by treating them in a furnace at 1675°F (913°C) for one hour and air cooling.

Twelve transverse CVN specimens and duplicate transverse 0.357-inch-diameter (9.07 mm) tension-test specimens were machined from the quarter point of each of the plates. The CVN specimens were tested over a range of temperatures to establish transition behavior. The tension specimens were tested at room temperature.

Gleeble Treatment

A Gleeble instrument was used to cycle slightly oversized Charpy blanks through simulated high-heat-input welding cycles. The temperatures simulated are those in one-inch base plate 1 mm from the fusion line for both a 1000 kJ/in. (40 kJ/mm) electroslag weld (ESW) cycle, and a 180 kJ/in. (7 kJ/mm) submerged-arc weld (SAW) cycle. The cycle temperatures, as determined in Phase II, are set out in Appendix A and illustrated in Figure 2. Eight CVN samples were prepared for each weld-cycle simulation.

Five steels from this program were subjected to a modified ESW cycle. This cycle was identical to the normal cycle during the heating phase and the initial part of the cooling phase. However, during the later stages of cooling the specimen blanks were water quenched from a series of temperatures in the range 1292°F (700°C) to 662°F (350°C). CVN specimens were made from blanks treated by these interrupted cycles for testing and microstructural evaluation.

Welding

Two steels with the most promising compositions were selected for welding trials. All weld passes were made in a longitudinal direction. Plate samples of each of the steels were electroslag (ES)-welded at a heat input of about 1000 kJ/inch and submerged-arc (SA)-welded in two passes at a heat input of 180 kJ/inch per pass and in six passes at a more typical heat input of 75 kJ/inch (3.0 kJ/mm). The joint configurations and welding conditions are shown in Figure 3, and typical chemical compositions of the electrodes are given in Table III.

CVN specimens were machined from the weldments in accordance with ABS and USCG qualification requirements. The CVN specimens were machined from the plate quarter thickness perpendicular to the weld-pass direction with the notch normal to the plate surface and located at the fusion line and in the HAZ at distances of 1 and 3 mm from the fusion line (positions b, c, and d in Figure 4). Because the fusion line was rarely perfectly

perpendicular to the plate surface over the entire thickness of the CVN specimen, different portions of the notch were generally at different distances from the fusion line. Quadruple tests were conducted at 0 and -40°F (-18 and -40°C) for each of the these three locations.

Microstructures and Fractography

Samples of the base plate and of the HAZ's (real and simulated) of all steels were examined by light microscopy to determine grain size and the distribution of transformation products. Carbon extraction replicas were obtained from the base plate and the HAZ of selected steels to determine the size and density of TiN precipitates by transmission electron microscopy. Fracture surfaces together with a polished section of the adjacent base metal were examined by scanning electron microscopy.

Results

Base Plate Properties and Microstructures

The base-plate properties of seventeen steels are summarized in Table IV. The yield strength of the base plate was not markedly changed by the addition of titanium alone; values ranged from 40 to 48 ksi for the titanium steels. The transition temperatures also appeared independent of titanium content up to 0.03 percent. The addition of residuals alone improved base-plate strength and toughness. The addition of titanium with residuals had no effect on strength, but degraded toughness. This latter effect was also observed in Phase II[1)] and is presumed to result from TiN particles at grain boundaries. Vanadium alone or combined with residuals, titanium and nitrogen, or titanium and silicon strengthened the base plate and had little effect on base-plate toughness. Individual CVN test results are shown in Appendix B.

The microstructures of the normalized base plates consisted of fine, uniform polygonal ferrite (ASTM 8.5 to 9.5) and banded pearlite. Occasional patches of martensite (M) were

seen in the steels containing residuals or higher manganese. Typical base-plate microstructures are shown in Figure 5.

Simulated HAZ's

Table V summarizes the mechanical properties and the microstructures observed in the HAZ's of all the steels after simulated SAW and ESW cycles. The mechanical properties that are evaluated are the 50-ft-lb transition temperature, Rockwell B hardness, and the fracture-appearance transition temperature (FATT). The 50-ft-lb transition temperature was selected because the 20-ft-lb transition temperature normally used for ship steels is near the lower shelf where the CVN data are scattered and more difficult to evaluate. Nevertheless, the conclusions drawn from the trends in both transition temperatures are similar. The individual CVN data are shown in Appendix C. The microstructural parameters relevant to HAZ properties are the prior austenite grain size, the morphology of the ferrite and the type of microconstituents present (pearlite, bainite, or martensite). Microstructures of the HAZ's of all the steels after simulated SAW and ESW cycles are shown in Figure 6. The tabulated data (Table V) are divided into three steel groups. The first group contains the base steel (without residuals) with microalloying additions of titanium and nitrogen. The steels with residuals and titanium additions make up the second grouping, and vanadium steels with titanium and nitrogen additions make up the third set.

In Figure 7, the 50-ft-lb transition temperature and the 50 percent shear transition temperature are used to distinguish the performance of all of the Phase III steels. Here the CVN data are plotted and grouped into good, fair, and poor regions. Four steels fall in the good category for both cycles and both transition temperatures; these are T7, T8, T1, and T10. The poor category is made up of the vanadium steels and the residual steel. The rest fall into the "fair" group. Each group of steels was examined in detail to determine the influence of composition and microstructure on toughness.

In the first group of steels the effect of titanium and nitrogen additions on the base steel can be determined. Steels T8 and T10 are microalloyed with low levels of titanium and nitrogen. After the simulated SAW cycle, the 50-ft-lb transition temperature of the HAZ of these steels was lower (better) than that of the base steel. After the simulated ESW cycle, the transition temperature of the HAZ of these steels was similar to that of the base steel. There were no trends evident in FATT of the HAZ's of this group of steels. The prior austenite grain size of the HAZ of the low-titanium steels was refined slightly relative to that of the HAZ of the base steel after the SAW cycle, but little change was noted after the ESW cycle. This would suggest that the grain boundary pinning effect of TiN precipitates is minimal for very high heat input welds when the microalloying additions of titanium and nitrogen are small. The effect of the titanium and nitrogen additions on the microconstituents in the HAZ is to promote pearlite formation at the expense of lower temperature transformation products. It is interesting to note that the higher manganese content in T8 (as compared to T10) resulted in slightly more martensite in the HAZ with consequently slightly poorer HAZ toughness after the SAW simulation.

At higher levels of titanium and nitrogen (steels T1, T7 and T11) the 50-ft-lb transition temperature of the HAZ was significantly lower than that of the base steel after the ESW cycle, but no different after the SAW cycle. The prior austenite grain size of the HAZ after simulated welding cycles was reduced for steels T1 and T7, but not for T11. All these steels have a mixed equiaxed-Widmanstatten ferrite morphology with pearlite as the only other constituent present. It is interesting to note that for steels with these higher levels of titanium and nitrogen, when the manganese level was raised (without altering the transformation products), the 50-ft-lb transition temperature was lowered (improved).

Steel T9 with higher manganese and silicon did not perform well in CVN tests for either cycle. This poor performance was due to the presence of martensite as a constituent in the HAZ.

Steels T2 and T3 had the highest levels of titanium and nitrogen. These steels had high CVN transition temperatures, even though they had small prior austenite grain sizes in the HAZ's and mixed equiaxed-Widmanstatten ferrite with pearlite as transformation products. The poor performance of these steels with desirable microstructures will be discussed later.

An illustration of the influence of titanium and nitrogen in changing the ferrite morphology and the microconstituents of the HAZ of these steels is shown in Figure 8. These microstructural changes had a pronounced effect on the transition temperature and on the form of the fracture transition curve. In Table VI the 50-ft-lb transition temperatures for the HAZ's of steels in Phase III (excluding the high nitrogen steels) are arranged according to the microconstituents observed after the SAW and ESW cycles. In general superior performance was observed when pearlite was the major microconstituent with at most a minor amount of martensite. The presence of appreciable martensite caused significantly poorer toughness; the 50-ft-lb transition temperature averaged 60°F higher.

The effect of the change in ferrite morphology on the form transition curve is illustrated in Figure 9. The equiaxed ferrite and pearlite that exists in the titanium steels gave rise to an abrupt transition between the upper and lower shelves. HAZ's containing Widmanstatten ferrite with more finely dispersed lenticular islands of pearlite and martensite showed a gradual increase in energy absorption with increased temperature. These results can be understood in terms of a model similar to that suggested by Pickering[2)] that deals with ease of crack propagation through ferrite-carbide mixtures. Although cracks are more difficult to initiate in the equiaxed-ferrite-pearlite

titanium steels (i.e., they initiate at lower temperatures), the widely spaced ferrite-carbide aggregates offer little impediment to crack growth once the cracks have formed. On the contrary, the finer dispersions of martensite in the titanium-free steels initiate cracks at higher temperatures. However, these are blunted by the ferrite plates so that growth proceeds by a start-stop mechanism through alternate layers of martensite and ferrite. Thus, high temperature toughness is lower in the titanium-free steels, but the transition is spread out over a broad temperature range so that at low temperatures, the titanium-free steels may actually have higher toughness than the titanium steels (compare B and T2 in Figure 9).

The second group of steels (R, T4, T6 and T5) demonstrate the effect of titanium and nitrogen on the properties and microstructures of the HAZ's of residual-bearing steels. The plain residual steel (R) had high CVN transition temperatures. The prior austenite grain size in the HAZ was coarse and the transformation products consisted of Widmanstatten ferrite and martensite (with minor amounts of pearlite).

In steel T4 moderate levels of titanium and nitrogen had been added to the residual steel. The 50-ft-lb transition temperatures of the HAZ's (particularly for the ESW steels) were lowered by these additions. However, even with titanium nitride precipitation, the prior austenite grain size in the HAZ was coarse. The transformation products were more desirable than those of the plain residual steel in that pearlite was more abundant and the ferrite morphology was less acicular.

In steels T6 and T5 the effects of lowering the manganese level and residual level are seen. The results for steel T6 were somewhat puzzling. The effect of the lower manganese level in steel T6 was to raise the CVN transition temperature relative to steel T4 despite the somewhat superior transformation products in steel T6. The results for steel T5 were also puzzling. After the SAW simulation, the CVN transition temperature of the HAZ was slightly lower than that of steel T4

(with higher residuals) as one might expect. The toughness of the HAZ after the ESW simulation, however, was worse because the transformation products in this steel after ESW simulation were primarily martensite and bainite.

The final group of steels all contained vanadium. The plain vanadium steel V1 had a slightly higher CVN transition temperature than the base steel. It had a coarse prior austenite grain size containing Widmanstatten ferrite with mostly pearlitic microconstituents. The addition of residuals to the vanadium steel caused the CVN results to deteriorate mostly due to the presence of martensite in the HAZ. The last two steels in the vanadium group, steels VT and VTN, had very high CVN transition temperatures. The reason for the poor performance of steel VT was the presence of martensite as a microconstituent in the HAZ. Steels VTN had a desirable microstructure in the HAZ with a small prior austenite grain size and ferrite-pearlite microconstituents. As with steels T2 and T3, the high nitrogen content was responsible for the poor performance of steel VTN.

Fracture-Path Studies

The CVN impact specimen fracture surfaces were examined using a technique that permits the simultaneous observation of the fracture surface and the etched microstructure adjacent to the fracture.

Figure 10 shows the fracture surface and etched microstructures from three steels (T1, T2 and VTN) broken at 0°F (-18°C). Steel T1 is a relatively low nitrogen steel, and steels T2 and VTN are high nitrogen steels. There was no secondary cracking observable adjacent to the fracture surface of the low nitrogen steel (T1). However, in the high nitrogen steels secondary cracking in ferrite was observed. This is indicative of low ductility in the ferrite and contributes to the high CVN transition temperature of the HAZ's of these steels. If the fracture is examined near the ductile region close to the notch, matrix deformation on the etched surface is visible in the low nitrogen steel. For the high nitrogen steels, virtually no

deformation of the etched microstructure is observable near the notch. The effect of high nitrogen in reducing the ductility of the HAZ ferrite is the chief reason for the poor performance of the high nitrogen steels.

The Roles of N and TiN

It was observed that the low temperature toughness of the HAZ was improved by small additions of titanium and nitrogen, but that higher levels of these elements were detrimental to HAZ toughness. Table VII summarizes the nitrogen distribution and toughness for the base steel and the five steels containing only titanium and nitrogen additions. The precipitated nitrogen was calculated based on the assumption that during cooling after the SAW and ESW cycles all of the titanium combines stoichiometrically with nitrogen to form TiN. The soluble nitrogen is the difference between total and precipitated nitrogen. Figure 11 shows the relation between the 50-ft-lb transition temperature and both precipitated and soluble nitrogen. There is an optimum level of precipitate that minimizes the transition temperature for each cycle: 20 ppm N (~0.006 Ti) for the SAW cycle and 40 ppm N (~0.013 Ti) for the ESW. Furthermore, there appears to be a general rise in transition temperature with increase in soluble nitrogen. However, because the soluble and insoluble fractions increase concurrently in these steels, it is difficult to assess accurately the separate contributions of these two forms of nitrogen.

There is also evidence of re-solution and ripening of the TiN precipitate during the weld cycles which further complicates any such analysis. Table VIII shows the average TiN and precipitate size for steels containing three levels of titanium and nitrogen (Ti/N) after normalization, and after SAW and ESW cycles. The TiN precipitates were measured by an extraction replication technique. The TiN was differentiated from AlN because of its cuboid shape. Clearly, the simulated weld cycles caused growth of the TiN particles. However, with the exception of the low Ti/N steel (T10) in which all the particles dissolved

in the ESW cycle, the remaining particles were still below the critical size of 50 nm that is necessary, according to Kanazawa,[3] to pin grain boundaries in the HAZ. Nevertheless, such growth during weld simulation required some dissolution of the particles that were present in the normalized steels so that the effective levels of soluble and precipitated nitrogen in the HAZ were unknown.

Table VIII also shows an apparent inverse relation between TiN particle size and the Ti/N concentration. This occurs because the very coarse precipitates that formed in the melt of the medium and high Ti/N steels were too widely spaced to be counted on extraction replicas. They were sufficiently dense, however, to act as nuclei on which titanium and nitrogen precipitated during ingot cooling. Only at relatively low temperatures, where the diffusion rate is too low to allow transfer to the coarse particles, did the titanium and nitrogen atoms nucleate a fine dispersion of TiN particles. It is this fraction of a bimodal distribution that was measured by TEM.

The effect of TiN particle size on the degree of grain coarsening in the HAZ was studied by artificially aging Gleeble specimens prior to the weld simulations. Samples of the high Ti/N steel T3 were aged for periods of up to 200 hours at 2192°F (1200°C). The growth of TiN particles during these treatments is shown in Figure 12. Particle diameter increased linearly with the cube root of time as predicted.[4] Samples with four different particle sizes were exposed to the ESW simulation. The grain sizes that developed in the HAZ's of these samples are shown in Table IX. As can be seen, an increase in particle diameter by a factor of 10 to 20 caused an increase in grain size of only 0.5 ASTM number (i.e., from 215 to 255 μm). The CVN impact values were not altered after annealing to produce larger TiN particle sizes. This would suggest that rapid solidification by continuous casting to produce a fine TiN size may not be necessary to produce good HAZ properties.

Development of the Transformation Products

The development of the transformation products during cooling between 1292°F (700°C) and 662°F (350°C) in the ESW cycle was examined for six steels, Figure 13. This was done by water quenching the specimens from various temperatures while cooling through the transformation temperature regime. Grain-boundary ferrite (GBF) began to form in all the steels between 1247°F (675°C) and 1202°F (650°C). From the grain boundary allotriomorphs, Widmanstatten side plates began to develop between 1202°F (650°C) and 1157°F (625°C) in all the steels except the high-Ti/N steel (T3). In the base (B) and residual (R) steels, the side plates continued to grow to fill the grain interiors during further cooling down to between 977°F (525°C) and 932°F (500°C), Figure 14. In the low Ti/N steels, side plate development was slightly less than for the base (B) or residual (R) steels. In the medium Ti/N steels with and without residuals (T4 and T7), side-plate growth was quickly blunted, and this form was replaced by equiaxed or blocky ferrite that nucleated principally in the grain interiors until the prior austenite grains were filled. Formation of the equiaxed ferrite was promoted by further increase in TiN so that only this morphology formed in the high Ti/N steel (T3) to the exclusion of the Widmanstatten plates. Formation of equiaxed ferrite started at ~1202°F (650°C), and had completely filled the grains by 1067°F (575°C), Figure 14.

Pearlite began to form in the carbon-rich austenite at 1112°F (600°C) to 1067°F (575°C) in the residual-free steels, but not till 1022°F (550°C) to 887°F (475°C) in the residual steels, Figure 14. In the base and low Ti/N steels (B and T10), the pearlite reaction was ~70 percent complete at 797°F (425°C). Pearlite formation was promoted in the higher Ti/N steels so that it was ~60 percent complete at 1022°F (550°C) in the medium Ti/N steel (T7) and fully complete at that temperature in the high Ti/N steel (T3). By contrast, in the residual steel (R), the pearlite reaction was only ~50 percent complete at 602°F (350°C). The addition of titanium to the residual steel (T4)

again promoted completion of pearlite formation, raising the pearlite-finish temperature to 752°F (400°C), Figure 13.

Specimens of four steels with dissimilar transformation behaviors (the low and high Ti/N steels [T10 and T3], and the residual and residual plus titanium steels [R and T4]) that had been quenched from various temperatures in the cooling portion of the ESW cycle were Charpy tested at 122°F (50°C) to determine at what point in the development of their transformation products full shear behavior toughness in the Charpy test was achieved. The fraction of full toughness (the ratio of energy absorbed after quenching to that at the completion of the full cycle) versus quench temperature is plotted in Figure 15 for quench temperatures down to 662°F (350°C). The high Ti/N steel (T3) that was fully transformed at 1022°F (550°C) achieved full toughness after quenching from between 1062°F (575°C) to 1022°F (550°C), whereas the low Ti/N steel (T10), which was slower to transform, did not achieve full toughness until it was quenched from ~842°F (450°C). The residual steel (R), whose transformation was incomplete even at 662°F (350°C), never achieved full toughness after quenching. The addition of titanium to the residual steel (T4) caused transformation to be complete at 762°F (400°C), and therefore, this steel achieves full toughness after quenching from between 752°F (400°C) and 662°F (350°C).

Weldments

Two steels (T10 and T11) containing the most promising ranges of titanium (0.006 and 0.013%) and nitrogen (0.003 and 0.005%) were rolled to 1-inch-thick (25.4 mm) plate for welding trials at three heat inputs. Results of Charpy tests at 0 and -40°F on specimens from three distances from the fusion line are summarized in Table X. (All data are contained in Appendix D.) An examination of energy absorption in specimens at the 1 mm position shows that the lower Ti/N steel T10 (0.006%Ti/0.003%N) was consistently better than the higher Ti/N steel T11 (0.013%Ti/0.005%N). At the highest heat input (1000 kJ/inch) steel T10 had a CVN energy absorption of 35-ft-lb at -40°F

compared to 12-ft-lb for T11; under the same conditions at 0°C, T10 absorbed 82-ft-lb, T11 absorbed 54-ft-lb. Energy absorbed generally increased with decreasing heat input. Both steels appeared to be on the upper shelf at -40°F for the 75 kJ/inch welds.

The toughness results for the real weldments at the 1 mm point, although showing somewhat more scatter, were generally better than those of the Gleeble-simulation specimens. Table XI compares the toughness results and microstructures of the real and simulated HAZ's. The energy absorption was higher in the real HAZ's of both steels for both the 180 kJ/inch SA and the 1000 kJ/inch ES welds. This appeared to be more a result of the differences in the widths of the HAZ produced by the two procedures than to microstructural differences in the HAZ. The real weld HAZ was narrower and was rarely a well defined band perpendicular to the plate surface, Figure 16. Consequently the Charpy specimen crack was located in coarse- and fine-grained material. The corresponding crack in the very broad HAZ of the Gleeble simulation was located in only coarse-grained material.

The microstructures within the coarse-grained HAZ's of real and simulated welds were only slightly different, Table XI. The grain sizes in the HAZ's in the real SA weldments were smaller than those in the HAZ's of the SAW simulation specimen, but the grain sizes were the same for the HAZ's of both real and simulated ESW procedures. The ferrite morphologies were very similar for the HAZ of specimens of both procedures, being mixtures of equiaxed and Widmanstatten ferrite in all but one case. The HAZ's of the real SAW specimens contain somewhat more bainite than do the corresponding simulation specimens, but this appeared to have no adverse affect on toughness. The micro-constituent of the HAZ of real and simulated ESW specimens was pearlite in all cases. These microstructures are summarized in Figure 17.

Discussion

The improvement in HAZ toughness caused by moderate-to-high titanium and nitrogen additions is partly due to the reduction in prior austenite grain size caused by the grain boundary pinning by TiN particles, but is primarily due to change of the ferrite morphology that alters the microconstituents formed during transformation. For low levels of nitrogen, titanium and aluminum act conjointly to getter free nitrogen[8] which also improves HAZ ductility.

After the formation of the grain-boundary allotriomorph, Widmanstatten side plates normally grow into the austenite grain interiors along planes of good fit between the austenite and ferrite (the low energy, Kurdjumov-Sachs [K-S] related planes). Growth occurs by migration toward the plate tip of high-mobility ledges climbing along the immobile K-S related planes.[5] The high aspect ratio of this form of ferrite results from the high ratio of the rate of ledge migration to the rate of ledge generation. In titanium steels, the TiN particles interact with the ledges and impede their motion, thereby reducing the aspect ratio toward that of blocky ferrite. The resultant slower growth of the plates from grain boundary to grain interior allows time for additional nucleation of ferrite within the austenite grains (perhaps at TiN particles), thereby reducing the grain size of the ferrite. Thus, TiN particles alter both the size and shape of the ferrite (Figure 8) by a mechanism shown schematically in Figure 18. This morphology change due to TiN particles is most important for moderate-to-high levels of titanium and nitrogen additions.

The TiN-induced change in ferrite morphology alters the size and shape of the remaining austenite pools, but electron microprobe analyses revealed no differences in carbon and manganese concentrations. In the base steel and the residual steel, the rapidly-growing Widmanstatten plates continue to subdivide the austenite pools into fine, lenticular plates, Figure 8. These plates contain few of the high-energy ledges

that are preferred over the K-S related boundaries as pearlite nuclei. Consequently, at the rates of cooling used in these studies 180°F/min. (100°C/min.) to 342°F/min. (180°C/min.), the austenite in the base steel tends to transform to lower-temperature products (bainite and martensite), especially in the presence of residual elements (Cu-Ni-Cr-Mo). The blocky ferrite in titanium steels produces larger pools of austenite (Figure 8) containing a higher density of TiN-stabilized ledges on the ferrite-austenite boundaries. The austenite pools are fully formed and stable at 1067°F (575°C) and their sessile ledges act to nucleate pearlite at relatively high temperatures. Thus, despite the fact that microprobe data reveals that the carbon and manganese concentrations of the two types of austenite pools appeared to be the same, the transformation products vary from martensite, where the ledge density in the austenite pools is low, to pearlite, where the ledge density is high.

These results and the results of quenching studies of the development of the transformation products during cooling and their toughness clearly indicate a relationship between the presence of martensite as the minor microconstituent and poor toughness. (Similar observations have been made by Ikawa, et al.[6]) This relationship is apparent from an examination of Table VI, and from comparison of Figures 13, 14, and 15 which demonstrate that toughness develops only as martensite is eliminated as the microconstituent. Thus, HAZ toughness generally improves as hardenability is reduced by reducing residuals and by promoting the fine-grained, equiaxed form of ferrite through the use of TiN.

However, as demonstrated in Table VI and Figures 10 and 11, there is an exception to this relation between microstructure and properties. Steels used in this study and related studies that contained titanium and nitrogen in excess of 0.02 to 0.007, respectively, had poor HAZ toughness independent of microstructure, because nitrogen embrittled the ferrite. Thus, even in titanium steels, nitrogen levels must be kept low.

For very low levels of titanium and nitrogen additions, the effects of TiN particles on altering the shape of ferrite and prior austenite grain size in the HAZ is very much reduced because of the low particle density. In this case, the scavenging effects of titanium and aluminum in reducing the free nitrogen in the HAZ by forming TiN at high temperatures and AIN at low temperatures have the strongest influences in improving HAZ toughness.[8] The improved matrix ductility in the fracture path study is undoubtedly due to this effect.

The proposed steel (0.10 to 0.12 C, 1.3 to 1.6 Mn, 0.3 Si, 0.03 Al, 0.006 to 0.015 Ti) will meet a 40-ksi minimum yield strength requirement. Attempts to strengthen the matrix by solid-solution- or precipitation-hardening additions (Si, Cu, Ni, Cr, Al, V, and/or N) led to a deterioration of HAZ toughness after high-heat-input weld simulations. It is proposed, therefore, that if higher base plate strengths are required, they be achieved by variations in processing rather than composition, i.e., control rolling and accelerated cooling.

In summary, we can recognize three different mechanisms that alter the toughness of the HAZ in the steels under study here. For high levels of titanium and nitrogen additions, the TiN particle density and size is such that the austenite grain size in the HAZ is reduced relative to the base steel. The TiN particles, and possibly AlN precipitates, also interact with and pin ledges on Widmanstatten side plates. This allows time for intragranular nucleation to produce a more equiaxed ferrite, and it also promotes the nucleation of pearlite at the stabilized ledges. At intermediate levels of titanium and nitrogen additions, the TiN particle density is less effective in reducing the prior austenite grain size in the HAZ, but is still effective in altering the ferrite morphology and pearlite nucleation. Finally, for low levels of titanium and nitrogen additions, the prior austenite grain size is the same as that for the base steel and the ferrite morphology and pearlite nucleation at the ferrite-austenite interface are only slightly altered from the

base steel. For these steels, the scavenging actions of titanium and soluble aluminum in reducing free nitrogen contribute significantly to the improved ductility and toughness in the HAZ.

Conclusions

A steel containing (by weight percent) 0.10 to 0.12 C, 1.3 to 1.6 Mn, 0.3 Si, 0.03 Al, 0.006 to 0.015 Ti with low S (<0.005), N (<0.006), and residuals (Cu + Ni + Cr + Mo < 0.1) has shown excellent toughness in the HAZ of high-heat-input welds (CVN energy > 50-ft-lb at 0°F), and an average base plate yield strength of 40 to 48 ksi. Attempts to strengthen this steel by addition of vanadium, nitrogen, and silicon or the residuals (Cu, Ni, Cr, Mo) caused a degradation of HAZ toughness.

Two metallurgical factors contribute to poor HAZ toughness. High levels of nitrogen (>0.006%) promote crack growth by embrittling the ferrite matrix. As a consequence, nitrogen levels must be kept at or below 0.005 percent. Second, poor HAZ toughness is directly related to martensite content. Accordingly, hardenability agents should be kept at low levels, and titanium (~0.01%) should be added.

The improved HAZ toughness that was observed in titanium steels was attributed to the ability of a fine dispersion of TiN particles to reduce effective hardenability by: (1) pinning austenite grain boundaries, thereby inhibiting grain coarsening in the HAZ; (2) changing the morphology of the ferrite from grain-boundary nucleated Widmanstatten ferrite to intragranular-nucleated equiaxed ferrite; and (3) changing the minor transformation product from martensite to pearlite. The gettering action of titanium in lowering free nitrogen also improves HAZ toughness.

Recommendations

1. The best HAZ properties occur in the base steel with low nitrogen and a small Ti addition (0.006 to 0.01), which had

low base-plate strength in the normalized condition (yield strength 40-45 ksi). All attempts to strengthen the base plate by alloying resulted in a deterioration of HAZ toughness. Experience with similar steels indicates that yield strength can be raised by control rolling; such treatment would also improve base-plate toughness. Further strength increase would derive from accelerated cooling, which may allow for a reduction of carbon content and thus a further improvement in HAZ toughness.

2. Steels using TiN to inhibit grain coarsening are generally continuously cast to produce a fine TiN distribution. However, in the present work, the best HAZ toughness was obtained in steels containing lower-than-normal Ti and N levels in which TiN would not begin to precipitate until lower temperatures (e.g., 2400-2500°F for 0.006 Ti, 0.003 N) and thus may be relatively fine even in ingot cast product. Furthermore, recent work at NKK[8)] proposes that the importance of Ti (and Al) additions is to scavenge N and not to control microstructure. Thus, the size of the TiN particles may be unimportant; in fact, coarse particles would resist dissolution in the HAZ better than fines. Consequently, an examination of the effects of ingot cooling in low Ti/N steels with higher aluminum (0.05) is recommended.

We would suggest that these variables be examined on a laboratory scale before a decision is made on the composition and processing of a production heat.

References

1. B. G. Reisdorf and W. F. Domis, "Investigation of Steels for Improved Weldability in Ship Construction--Phase II," Ship Structure Committee Report No. SSC-305, 1981.
2. F. B. Pickering, "The Structure and Properties of Bainite in Steels," Transformation and Hardenability in Steels, Climax Molybdenum Co. of Michigan, Ann Arbor, 1967, p. 109.
3. S. Kanazawa, A. Nakashima, K. Okamoto, and K. Kanaya, "Improvement of Weld Fusion Zone Toughness by Fine TiN," Trans. ISIJ, Vol. 16, 1976, p. 486.
4. J. M. Lifshitz and V. V. Slyozov, J. Chem. Phys. Solids, Vol. 19, 1961, p. 35, and G. Wagner, Z. Electrochem., Vol. 65, 1961, p. 581.
5. H. I. Aaronson, "The Proeutectoid Ferrite and Proeutectoid Cementite Reactions," Decomposition of Austenite by Diffusional Processes, by V. F. Zackay and H. I. Aaronson, Interscience Publishers, New York, 1962, p. 387.
6. H. Ikawa, H. Oshige, and T. Tanoue, "Effect of Martensite-Austenite Constituent on HAZ Toughness of a High Strength Steel," Trans. Japan Weld. Soc., Vol. 11, 1980, p. 50.
7. S. Kanazawa, S. Saito, A. Nakashima, K. Yamato, K. Okamoto, K. Kanaya, and K. Tanabe, "High Tensile Steel for Large Heat-Input Automatic Welding and Production Process Therefore," U.S. Patent No. 3,773,500, Nov. 20, 1973.
8. M. Suzuki, M. Tsukada, and I. Watanabe, "Newly Developed Actic Grade High Al, Low N, Micro Ti Type Offshore Structural Steel," Proceeding of 2nd International Offshore Welded Structurals Conference, London, November 1982, Paper 16.

List of Tables

I Microstructures and Toughness of Five Steels from Phase II

II Chemical Composition of Steels Investigated, weight percent

III Typical Electrode Composition

IV Mechanical Properties of Normalized Base Plates--Transverse Orientation

V HAZ Microstructures and Toughness

VI 50-ft-lb Transition Temperatures for HAZ's with and without Martensite. ESW and SAW Cycles.

VII Relation Between Nitrogen and Toughness

VIII Average Size of TiN Particles in Three Titanium Steels Before and After Simulated Weld Cycles

IX Effect of TiN Particle Size on the Grain Size Developed in the ESW-HAZ of Steel T3

X CVN Energy of Weldments

XI Gleeble and Real Weld HAZ Toughness and Microstructures

Table I

Microstructures and Toughness of Five Steels from Phase II

Steel		Energy Absorbed at 0°F, ft lb		Prior Austenite Grain Size, ASTM		Transformation Products*			
						SAW		ESW	
Code	Type	SAW	ESW	SAW	ESW	Ferrite	Microconstituent	Ferrite	Microconstituent
2	Base	26	21	0.5	0.0	W	B + (P)	W	P + B
N	Ti	64	33	3.0	2.0	E	P + B	E + W	P
4	Residual	8	12	0.5	0.0	W	M + (P)	W	P
13	R + Ti	27	18	2.5	1.5	W + E	P + M	W + E	P
7	V	15	35	0.5	0.0	W	P + B	W	P

* W = Widmanstatten
E = Equiaxed
B = Bainite
P = Pearlite
M = Martensite
( ) = Minor amount

Table II

Chemical Composition of Steels Investigated, weight percent

Steel Code	Steel Type	C	Mn	P	S	Si	Cu	Ni	Cr	Mo	V	Ti	Al	N	B
B	Base	0.12	1.38	0.012	0.002	0.31	0.002	0.005	<0.003	<0.003	<0.002	<0.002	0.038	0.005	0.0005
	Titanium Steels														
T8	0.006 Ti + Mn	0.10	1.62	0.009	0.005	0.31	-	-	-	-	<0.002	0.005	0.037	0.003	<0.0002
T10	0.006 Ti	0.12	1.39	0.010	0.002	0.29	-	-	-	-	<0.002	0.006	0.059	0.003	<0.0002
T1	0.01 Ti	0.13	1.32	0.012	0.002	0.28	0.003	<0.002	<0.003	0.005	<0.002	0.011	0.042	0.006	0.0006
T7	0.011 Ti + Mn	0.13	1.58	0.012	0.002	0.29	0.003	<0.002	<0.003	0.005	<0.002	0.011	0.041	0.006	-
T11	0.013 Ti	0.12	1.32	0.010	0.002	0.27	-	-	-	-	<0.002	0.013	0.057	0.005	<0.0002
T9	0.006 Ti + Si + Mn	0.10	1.59	0.009	0.006	0.52	-	-	-	-	<0.002	0.007	0.056	0.004	<0.0002
T2	0.017 Ti + 0.01 N	0.13	1.34	0.010	0.002	0.30	0.003	<0.002	<0.003	0.004	<0.002	0.017	0.043	0.011	-
T3	0.030 Ti + 0.01 N	0.13	1.34	0.010	0.002	0.30	0.002	<0.002	<0.003	0.004	<0.002	0.030	0.039	0.011	-
	Residual Steels														
R	0.5 residuals	0.12	1.38	0.012	0.002	0.31	0.19	0.14	0.12	0.041	<0.002	0.003	0.036	0.005	-
T4	R + 0.016 Ti	0.13	1.35	0.012	0.002	0.30	0.19	0.15	0.14	0.042	<0.002	0.016	0.039	0.007	-
T6	R + 0.017 Ti - Mn	0.12	1.01	0.012	0.002	0.30	0.19	0.15	0.14	0.042	<0.002	0.017	0.039	0.006	-
T5	1/2 R + 0.016 Ti	0.12	1.37	0.012	0.002	0.31	0.11	0.073	0.066	0.022	<0.002	0.016	0.040	0.006	-
	Vanadium Steels														
V1	0.08 Vanadium	0.12	1.39	0.012	0.002	0.31	0.003	<0.002	<0.003	0.004	0.081	<0.002	0.039	0.006	-
V2	V + R	0.12	1.35	0.012	0.002	0.31	0.19	0.14	0.17	0.039	0.081	<0.002	0.037	0.007	0.0006
VT	V + 0.006 Ti + Si + Mn	0.10	1.58	0.009	0.006	0.54	-	-	-	-	0.060	0.006	0.053	0.004	<0.0002
VTN	V + 0.016 Ti + 0.01 N	0.12	1.36	0.011	0.002	0.29	0.003	<0.002	<0.003	0.004	0.084	0.016	0.039	0.011	0.0006

Table III

Typical Electrode Composition—Weight Percent

Electrode	Welding Process	C	Mn	Si	Cr	Ni	Mo	Cu
Armco W18	Submerged-arc	0.15	0.67	0.17	0.06	1.80	0.16	0.25
Linde M1-88	Electroslag	0.06	1.65	0.35	0.25	1.50	0.40	-

Note: Above is filler-metal manufacturer's data.

Table IV

Mechanical Properties of Normalized Base Plates--Transverse Orientation

Code	Steel Description	Tensile Properties: Yield Strength, ksi	Tensile Properties: Tensile Strength, ksi	Tensile Properties: Elongation in 1 Inch, percent	Toughness: 20-ft-lb TT, °F	Toughness: FATT, °F
	Titanium Steels					
B	Base	45.5	68.0	37.0	-115	-90
T8	0.006 Ti + Mn	47.0	68.5	36.0	-150	-40
T10	0.006 Ti	43.8	66.8	38.6	-100	-90
T1	0.011 Ti	45.2	68.7	37.0	-85	-70
T7	0.011 Ti + Mn	48.4	71.5	36.5	-90	-55
T11	0.013 Ti	39.2	65.1	39.4	-100	-90
T9	0.006 Ti + Si + Mn	49.6	71.2	36.5	-145	-85
T2	0.017 Ti + 0.01 N	48.7	69.8	37.5	-100	-65
T3	0.030 Ti + 0.01 N	46.1	69.1	37.0	-85	-40
	Residual Steels					
R	0.5 Residuals	48.4	71.8	36.0	-140	-110
T4	R + 0.016 Ti	49.0	71.8	35.5	-75	-70
T6	R + 0.017 Ti - Mn	44.5	66.8	37.0	-70	-55
T5	1/2R + 0.016 Ti	47.3	70.1	36.5	-90	-65
	Vanadium Steels					
V1	0.08 Vanadium	49.2	71.2	35.0	-90	-60
V2	V + R	55.5	77.8	32.0	-105	-65
VT	V + 0.006 Ti + Si + Mn	51.8	73.2	35.5	-150	-70
VTN	V + 0.016 Ti + 0.01 N	48.4	70.6	35.0	-110	-70

Table V

HAZ Microstructures and Toughness

Steels		Mechanical Properties						Microstructures					
		50-ft-lb TT, °F		FATT, °F		Hardness, HRB		Austenite Grain Size, ASTM		Transformation Products*			
										SAW		ESW	
Code	Type	SAW	ESW	SAW	ESW	SAW	ESW	SAW	ESW	Ferrite	Microconstituents	Ferrite	Microconstituent
B	Base	+15	+20	+40	+80	89	88	0	0	W	B + P	W	P + B
T8	0.006 Ti + Mn	0	+25	+45	+40	90	90	1.0	0	W	P + (M)	E	P + (M)
T10	0.006 Ti	-40	+25	+50	+50	96	94	0.5	0	W	P + (B)	E + W	P
T1	0.011 Ti	+15	+10	+30	+20	85	82	0.5	0.5	E + W	P	E	P
T7	0.011 Ti + Mn	0	0	+40	+30	86	91	1.0	1.5	E + W	P	E	P
T11	0.013 Ti	+10	0	+60	+60	97	92	0	0	E + W	P	E + W	P
T9	0.006 Ti + Si + Mn	+40	+55	+80	+80	93	90	1.0	0	W	P + M	W	P + M
T2	0.017 Ti + 0.01 N	+35	+65	+60	+70	88	80	1.0	1.0	E + W	P	E + W	P
T3	0.030 Ti + 0.01 N	+20	+60	+40	+70	86	78	1.0	1.5	E + W	P	E + W	P
R	0.5 Residuals	+70	+100	+120	+120	98	98	0	0.5	W	M + (P)	W	M + P
T4	R + 0.016 Ti	+45	0	+60	+50	98	88	0	0	W	P + (M)	E + W	P + M
T6	R + 0.017 Ti - Mn	+60	+40	+90	+40	88	87	0.5	0.5	E + W	P + (M)	E	P
T5	1/2 R + 0.016 Ti	+20	+45	+50	+40	92	93	0	0	W	P + B + M	W	M + B + P
V1	0.08 Vanadium	+40	+45	+80	+80	94	88	0	0.5	W	P + (M)	W	P
V2	V + R	+85	+120	+100	+120	95	93	0	0.5	W	P + M	W	P + M
VT	V + 0.006 Ti + Si + Mn	+70	+110	+80	+130	94	95	1.0	0	E + W	P + M	W	P + M
VTN	V + 0.016 Ti + 0.01 N	+70	+75	+100	+100	91	90	2.0	2.0	E	P	E	P

* E = Equiaxed
W = Widmanstatten
P = Pearlite
M = Martensite
B = Bainite
( ) = Minor amount

Table VI

50-ft-lb Transition Temperatures for HAZ's with and without Martensite. ESW and SAW Cycles

Steels		50-ft-lb Transition Temperature, °F	
Code	Type	Little or No Martensite	Appreciable Martensite
B	Base	+15	
		+20	
T8	0.006 Ti + Mn	0	
		+25	
T10	0.006 Ti	-40	
		+25	
T1	0.011 Ti	+15	
		+10	
T7	0.011 Ti + Mn	0	
		0	
T11	0.013 Ti	+10	
		0	
T9	0.006 Ti + Si + Mn		+40
			+55
R	0.5 Residuals		+70
			+100
T4	R + 0.016 Ti	0	+45
T6	R + 0.017 Ti - Mn	+60	
		+40	
T5	1/2 R + 0.016 Ti		+20
			+45
V1	0.08 Vanadium	+40	
		+45	
V2	V + R		+85
			+120
VT	V + 0.006 Ti + Si + Mn		+70
			+110
	Range	-40 to +60	+20 to +120

Table VII

Relation Between Nitrogen and Toughness

Steel	Total Titanium, wt%	Total Nitrogen, wt%	Nitrogen Partitioning Precipitated, ppm	Nitrogen Partitioning Soluble, ppm	50-ft-lb TT, °F SAW	50-ft-lb TT, °F ESW
B	<0.002	0.005	<6	>44	+15	+20
T10	0.006	0.003	18	12	-40	+25
T1	0.011	0.006	32	28	+15	+10
T11	0.013	0.005	38	12	+10	0
T2	0.017	0.011	50	60	+35	+65
T3	0.30	0.011	88	22	+20	+60

Table VIII

Average Size of TiN Particles in Three Titanium Steels Before and After Simulated Weld Cycles

Steel		TiN Particle Size, nm		
Code	Type	Normalized	SAW	ESW
T10	Lo TiN	25	40	*
T7	Med TiN	17	25	30
T3	Hi TiN	12	†	25

* All particles dissolved.
† Data not available.

Table IX

Effect of TiN Particle Size on the Grain Size Developed in the ESW-HAZ of Steel T3

TiN Particle Size, nm	HAZ Grain Size, ASTM
12	1.5
17	1.5
150	1.0
300	1.0

Table X

CVN Energy of Weldments

Steel	Weld	Heat Input, kj/inch	Position from Fusion Line, mm	CVN Energy, ft-lb 0°F	CVN Energy, ft-lb -40°F
T10	ES	1000	0	66	14
			1	82	35
			3	114	65
T11	ES	1000	0	25	17
			1	54	12
			3	116	64
T10	SA-2	180	0	43	38
			1	122	59
			3	186	129
T11	SA-2	180	0	72	23
			1	79	24
			3	153	150
T10	SA-6	75	0	164	149
			1	190	152
			3	171	138
T11	SA-6	75	0	150	105
			1	166	123
			3	168	138

Table XI

Gleeble and Real Weld HAZ Toughness and Microstructures

	Type	Code	CVN Energy, ft-lb* Test Temperature, 0°F SAW	CVN Energy, ft-lb* Test Temperature, 0°F ESW	CVN Energy, ft-lb* Test Temperature, -40°F SAW	CVN Energy, ft-lb* Test Temperature, -40°F ESW	Austenite Grain Size, ASTM SAW	Austenite Grain Size, ASTM ESW	Microstructures** SAW Texture	Microstructures** SAW Constituents	Microstructures** ESW Texture	Microstructures** ESW Constituents
Gleeble Samples	0.006Ti	T10	80	30	50	10	0.5	0	W	P + (B)	E + W	P
	0.013Ti	T11	50	50	10	10	0	0	E + W	P	E + W	P
Real Welds 1 mm from fusion line	0.006Ti	T10	122	82	59	35	2.0	0	E + W	P + B	E + W	P
	0.013Ti	T11	79	54	24	12	1	0	E + W	P + B	E + W	P

* SAW = 180 kJ/inch
ESW = 1000 kJ/inch

** E = Equiaxed
W = Widmanstatten
P = Pearlite
B = Bainite
( ) = Minor amount

List of Figures

1. Microstructures of the HAZ of the Residual Steel 4 (Top), and the Titanium Steel 14 (Bottom), from Phase II[1)]

2. Time-Temperature Cycles Experienced at the 1 mm Point in the HAZ of One Inch Thick Plate Welded by 180 kJ/inch SA and 1000 kJ/inch ES Processes

3. Joint Configuration and Weld Parameters Used in Current Investigation

4. Schematic of Notch Location for CVN Impact Specimens

5. Typical Microstructures of Base Plates from Phase III. Top, the Titanium Steel T6; Bottom, the Titanium plus Residual Steel T4.

6. Microstructures of the HAZ's of Steels in Phase III After Simulated SAW and ESW Cycles. 500X.

7. Ranking of Steels According to the 50-ft-lb and 50 Percent Shear Transition Temperatures in the HAZ of Simulated SAW and ESW Cycles

8. Ferrite Morphologies and Microconstituents in the ESW-HAZ of the Base Steel B (Top) and the High Ti/N Steel T3 (Bottom)

9. ESW-HAZ Energy Absorption Transition Curves Typical of Titanium Steels (T1, T2) and Titanium-Free Steels (B, R)

10. Fractographs of Charpy V-Notch Specimens Showing Cleavage Fracture in the Grain-Coarsened HAZ. (Gleeble Simulation of Electroslag Welding with 1000 kJ/inch Heat Input)—Phase III Steels Containing Titanium

11. Relation Between Soluble and Precipitated Nitrogen and the HAZ 50-ft-lb Transition Temperatures

12. Growth of TiN Particles with Time at 2200°F, Steel T3

13. Temperature Ranges in which Various Transformation Products Formed in Six Steels During Cooling from the ESW Cycle

14. The Development of Transformation Products in the HAZ of Three Steels (B, T3, R) During Cooling in the ESW Cycle. 100X.

15. Development of Toughness During Cooling from an ESW Cycle

16. Macrographs of Welds in Steels T11 and T10 at Three Heat Inputs: 1000 kJ/inch, 180 kJ/inch, and 75 kJ/inch

17. Microstructures in the HAZ of Welds of Steels T11 (Left) and T10 (Right) at Three Heat Inputs: 1000 kJ/inch ESW (Top); 180 kJ/inch SAW (Center); and 75 kJ/inch SAW (Bottom)

18. Growth of Ferrite: Top - in the Base Steel by Unrestricted Ledge Migration; Bottom - in a Titanium Steel Where Ledge Migration is Inhibited by TiN Particles

STEEL 4 X500

STEEL N X500

Figure 1. MICROSTRUCTURES OF THE HAZ OF THE RESIDUAL STEEL (4) TOP AND THE TITANIUM STEEL (N) BOTTOM FROM PHASE II.[1] 500X.

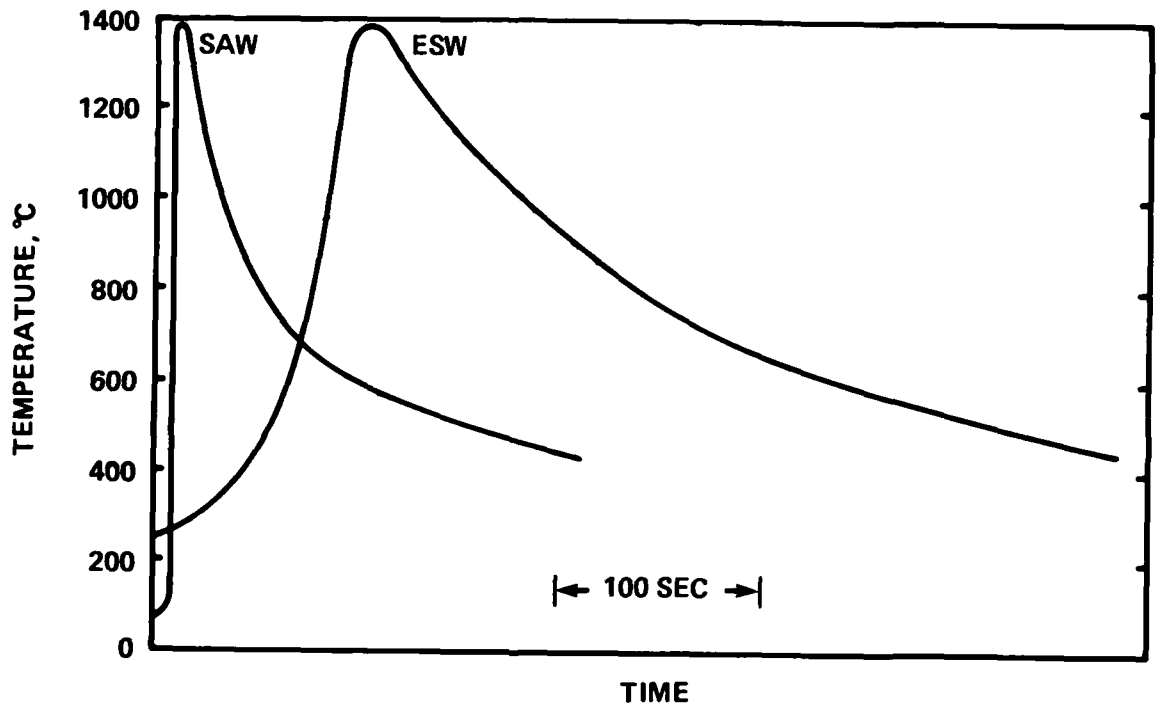

Figure 2. TIME-TEMPERATURE CYCLES EXPERIENCED AT THE 1mm POINT IN THE HAZ OF ONE-INCH PLATE WELDED BY 180 KJ/inch SA AND 1000 KJ/inch ES PROCESSES.
°F = 9/5°C + 32

RL-2-8396

SUBMERGED-ARC JOINT

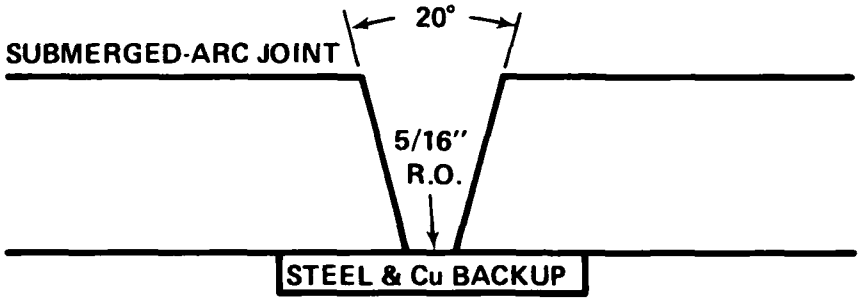

NORMAL-HEAT-INPUT SAW	HIGH-HEAT-INPUT SAW
ARMCO W18 ELECTRODE	ARMCO W18 ELECTRODE
LINCOLN 880 FLUX	LINCOLN 880 FLUX
600 AMPERES CURRENT	800 AMPERES CURRENT
32 VOLTS	30 VOLTS
15.5 IPM TRAVEL	8 IPM TRAVEL
6 PASSES—75 KJ/in. EACH	2 PASSES—180 KJ/in. EACH

ESW JOINT

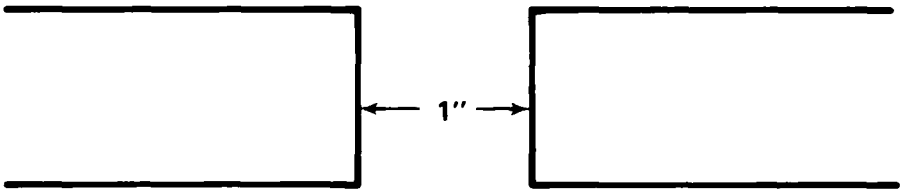

LINDE M188 ELECTRODE	37 VOLTS
LINDE 124 FLUX	120 IPM WIRE SPEED
450 AMPERES CURRENT	1 PASS—≈1000 KJ/in. EACH

Figure 3. JOINT CONFIGURATION AND WELD PARAMETERS USED IN CURRENT INVESTIGATION

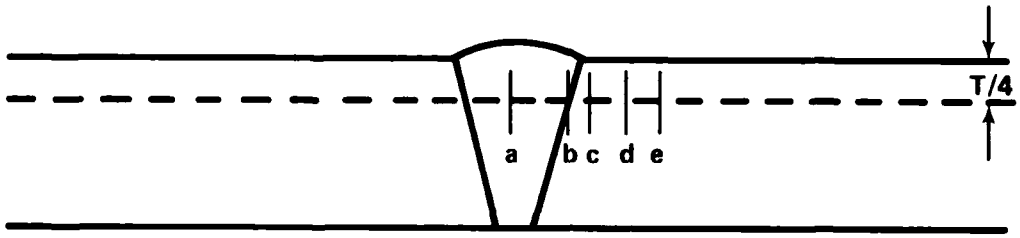

NOTCH LOCATION
- a - CENTER OF WELD
- b - FUSION LINE
- c - HAZ, 1 mm FROM FUSION LINE
- d - HAZ, 3 mm FROM FUSION LINE
- e - HAZ, 5 mm FROM FUSION LINE

Figure 4. SCHEMATIC OF NOTCH LOCATION FOR CVN IMPACT SPECIMENS

T6 X500

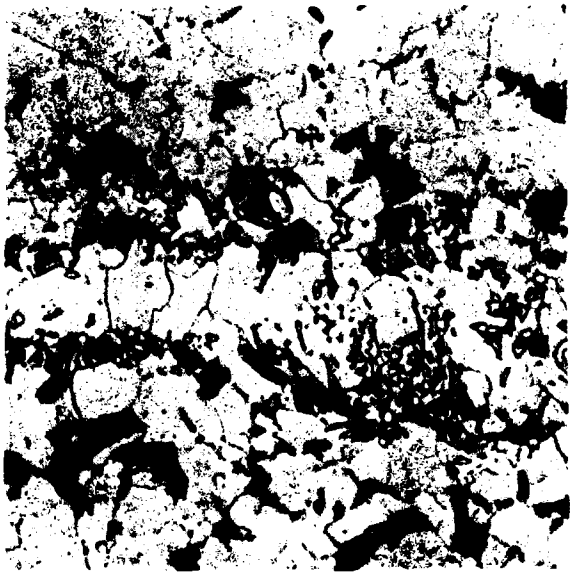

T4 X500

Figure 5. TYPICAL MICROSTRUCTURES OF BASE PLATES FROM PHASE III. TOP, THE TITANIUM STEEL T6; BOTTOM, THE TITANIUM PLUS RESIDUAL STEEL T4. 500X.

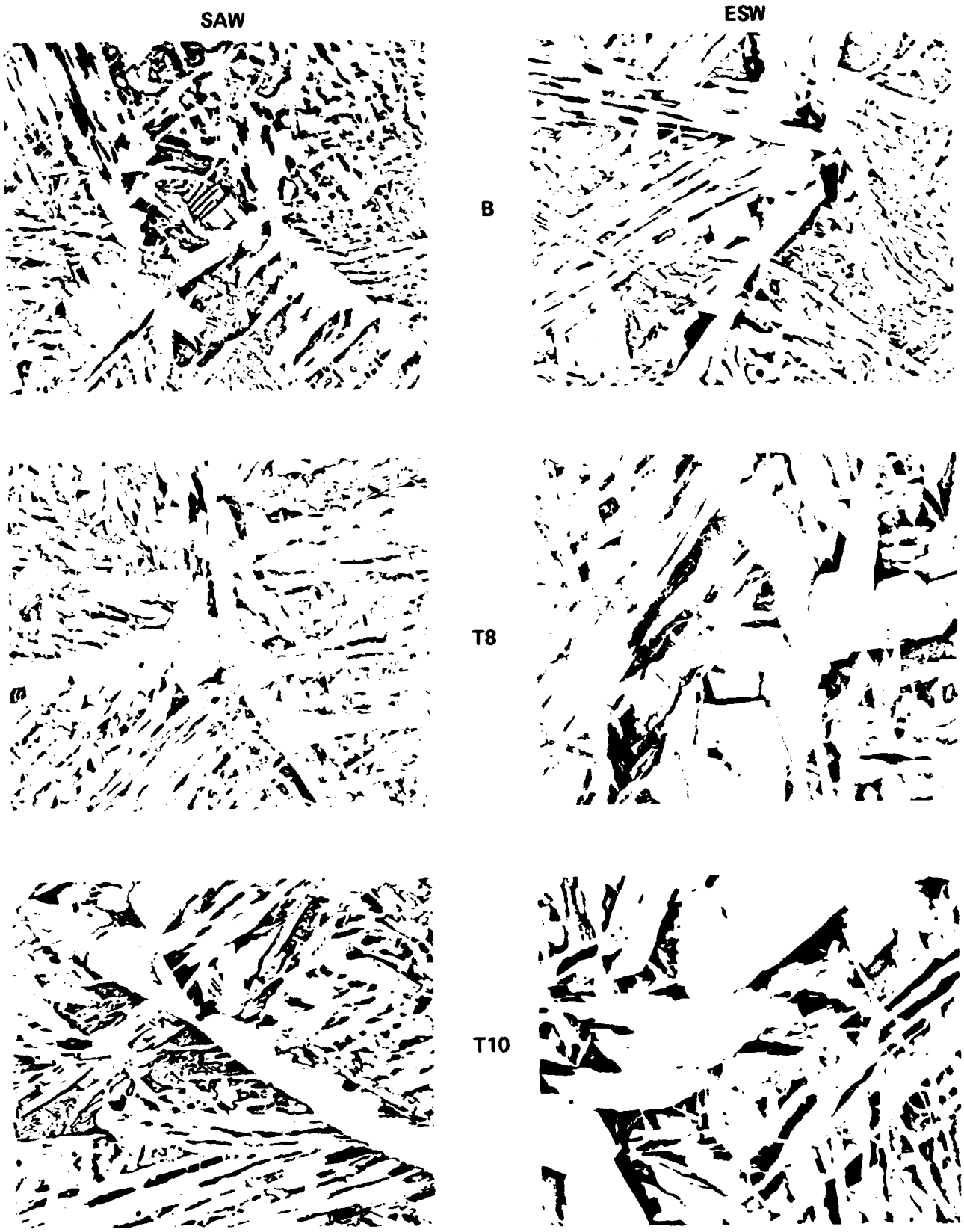

Figure 6. MICROSTRUCTURES OF THE HAZ'S OF STEELS IN PHASE III AFTER SIMULATED SAW AND ESW CYCLES. 500X.

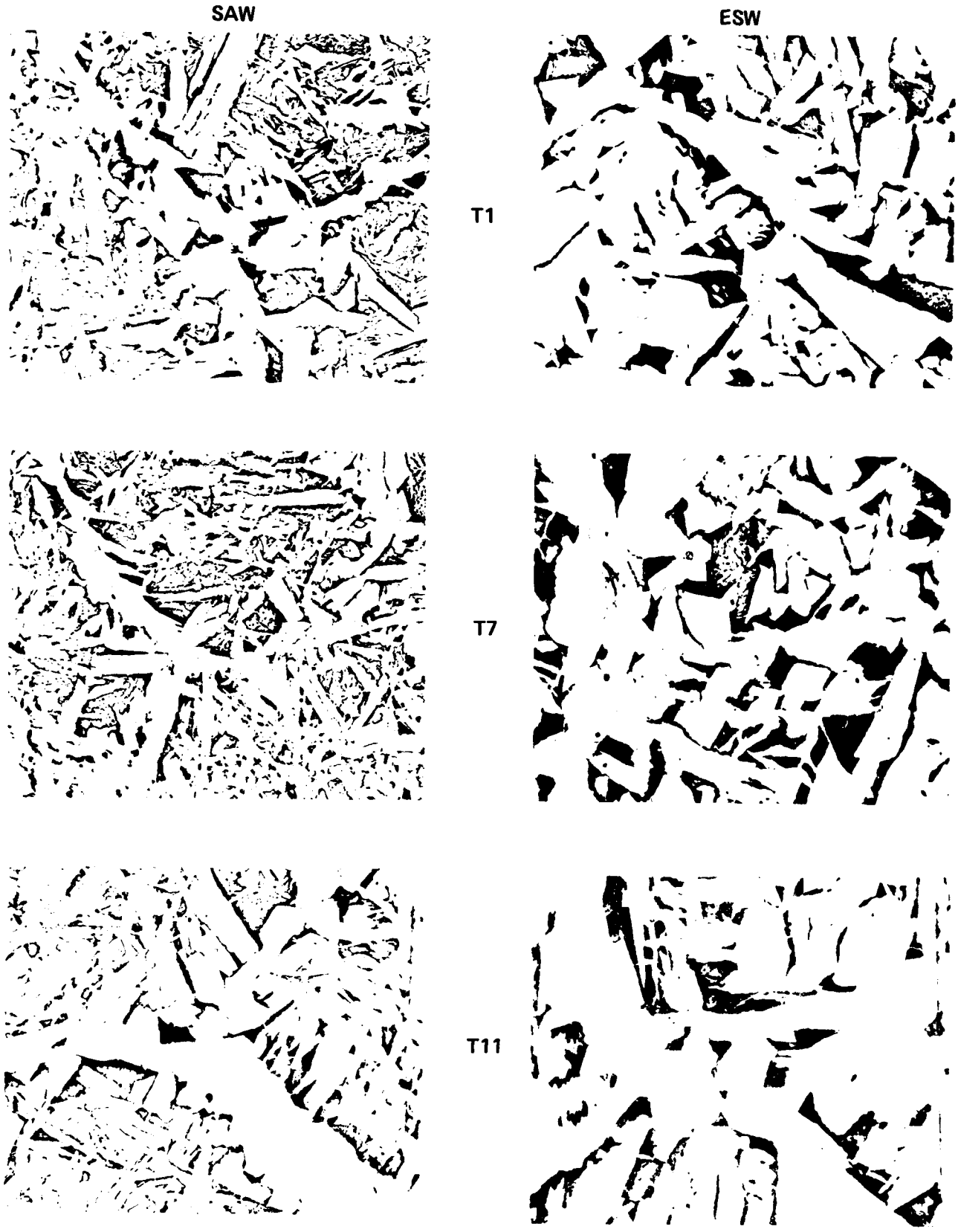

Figure 6. CONTINUED. 500X.

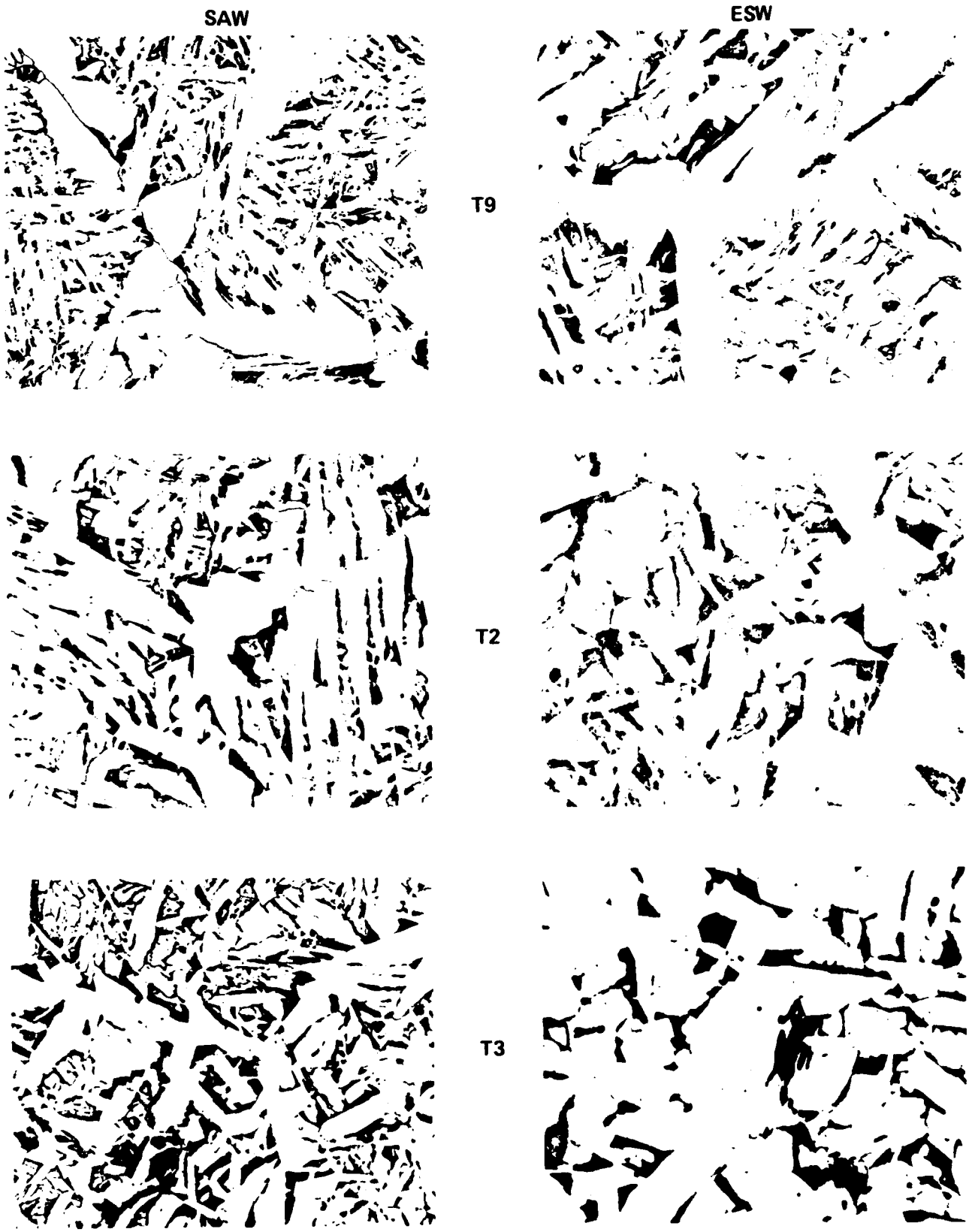

Figure 6. CONTINUED. 500X.

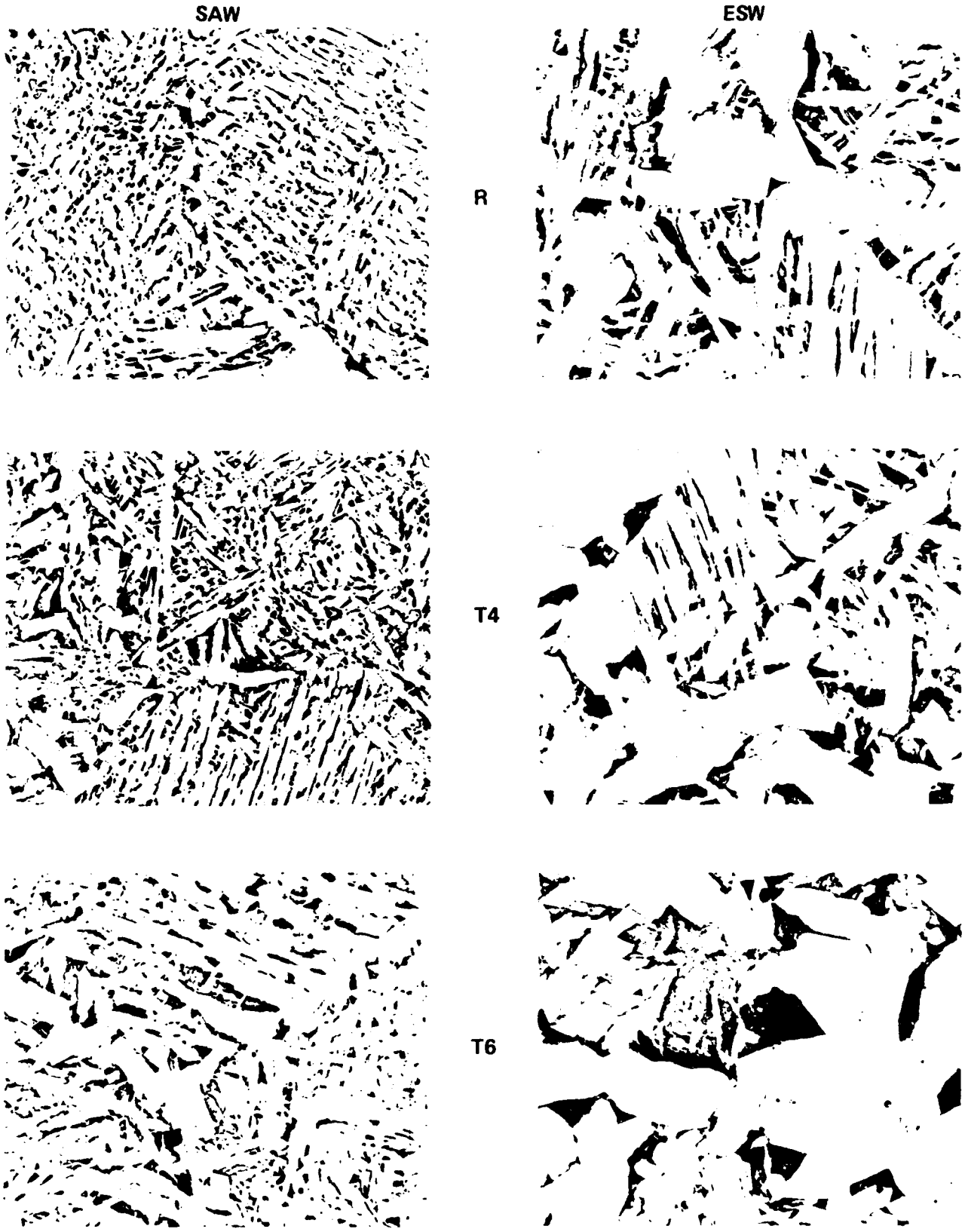

Figure 6. CONTINUED. 500X.

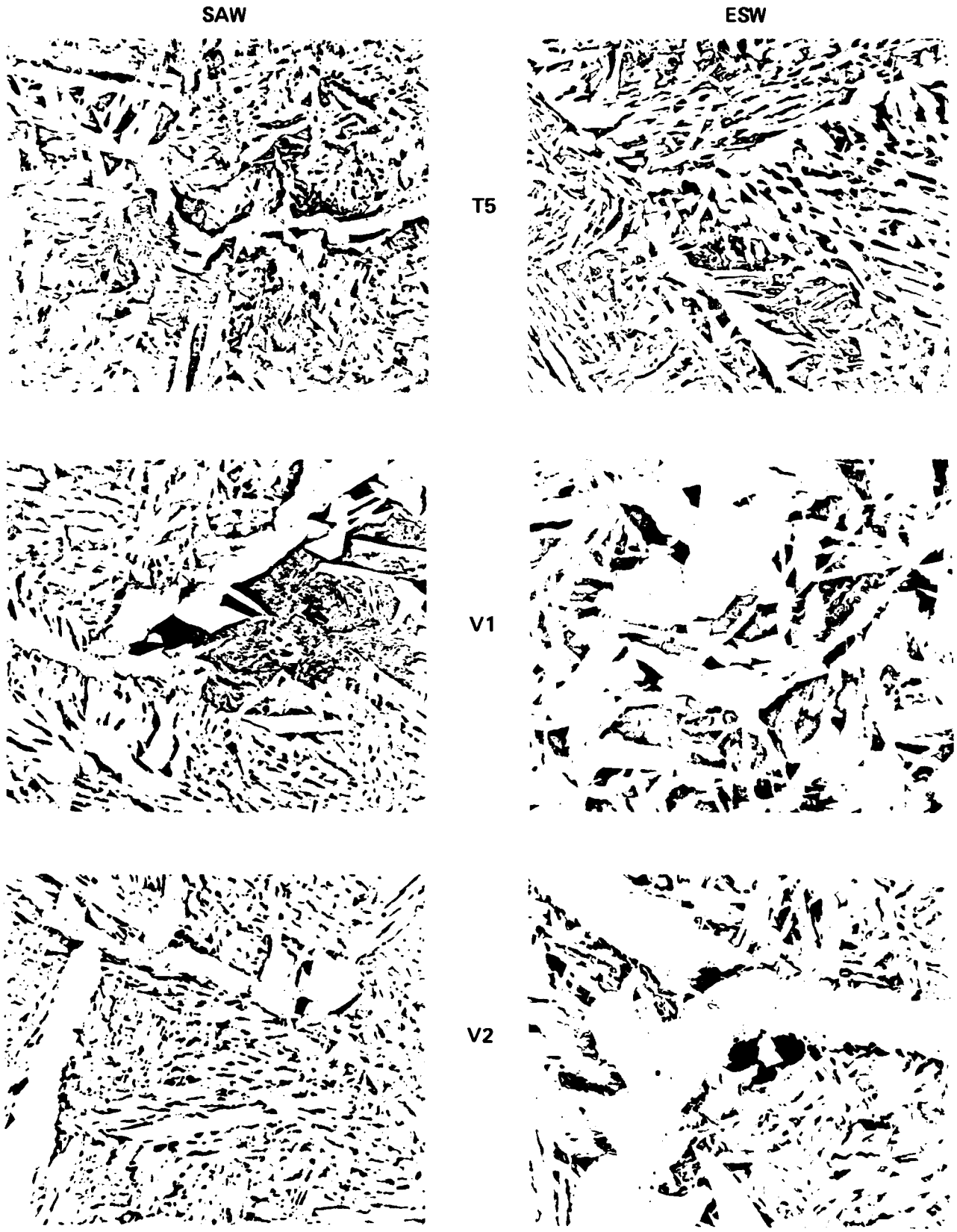

Figure 6. CONTINUED. 500X.

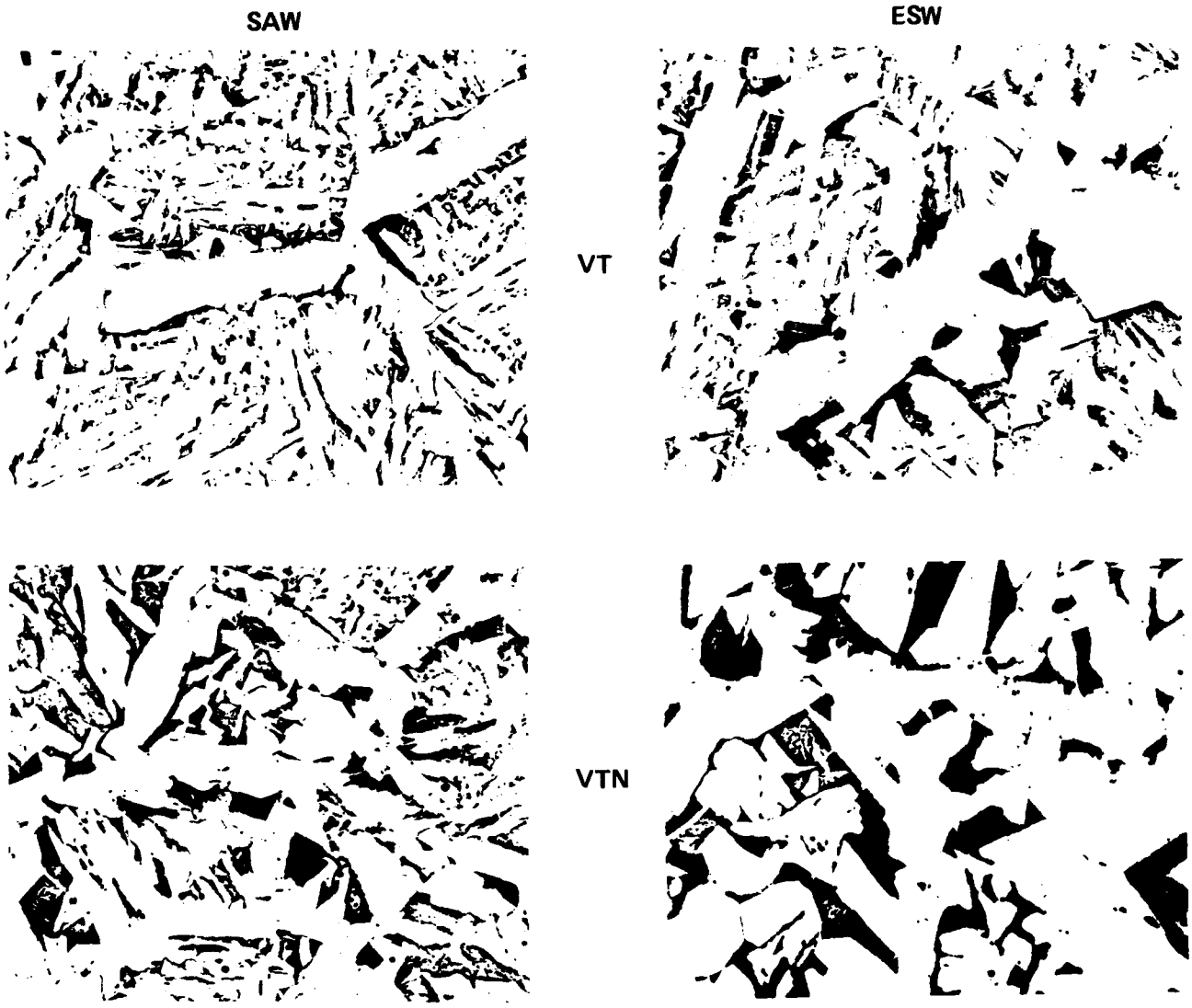

Figure 6. CONTINUED. 500X.

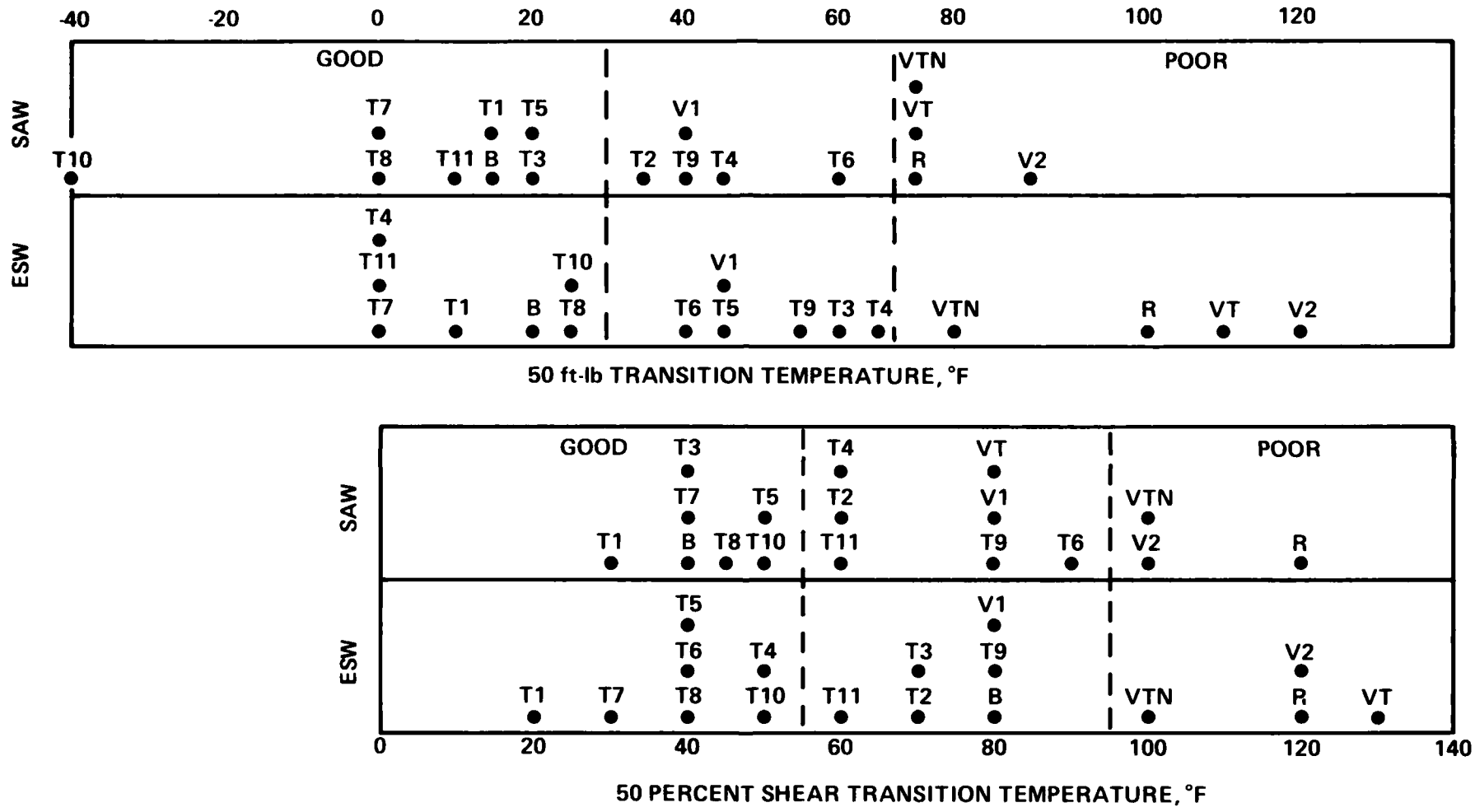

Figure 7. RANKING OF STEELS ACCORDING TO THE 50 ft-lb AND 50 PERCENT SHEAR TRANSITION TEMPERATURES IN THE HAZ OF SIMULATED SAW AND ESW CYCLES

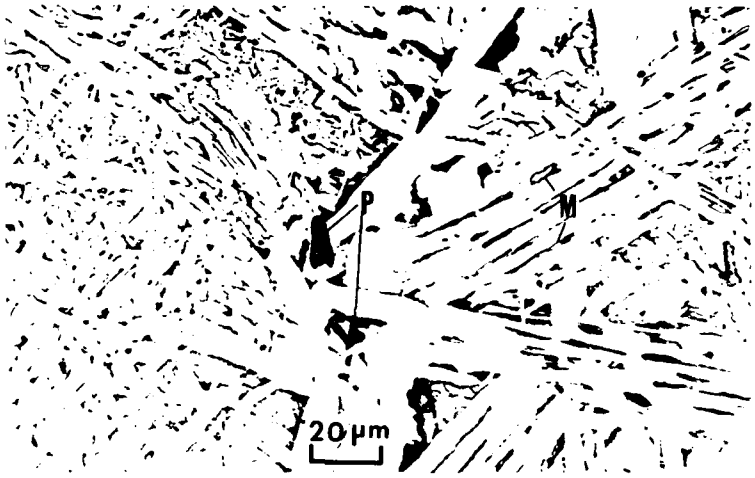

WIDMANSTATTEN FERRITE PLUS MARTENSITE (M) AND PEARLITE (P) IN THE BASE STEEL B

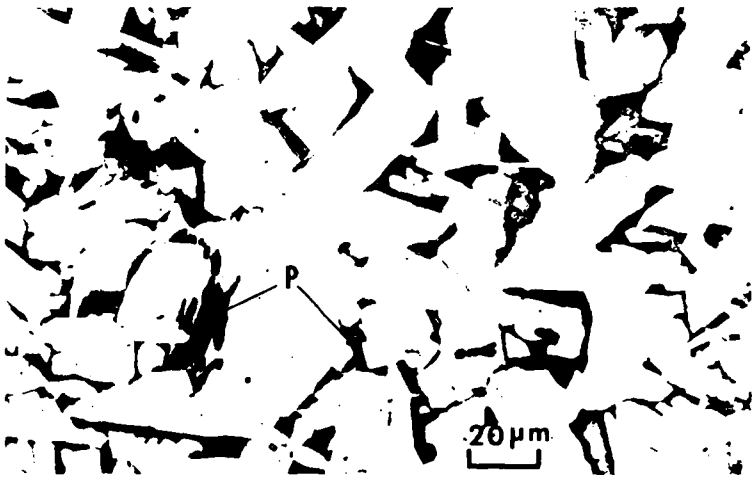

EQUIAXED FERRITE PLUS PEARLITE (P) IN THE HIGH-Ti/N STEEL T3

Figure 8. FERRITE MORPHOLOGIES AND MICROCONSTITUENTS IN THE ESW-HAZ'S OF THE BASE STEEL B (TOP) AND THE HIGH-Ti/N STEEL T3 (BOTTOM)

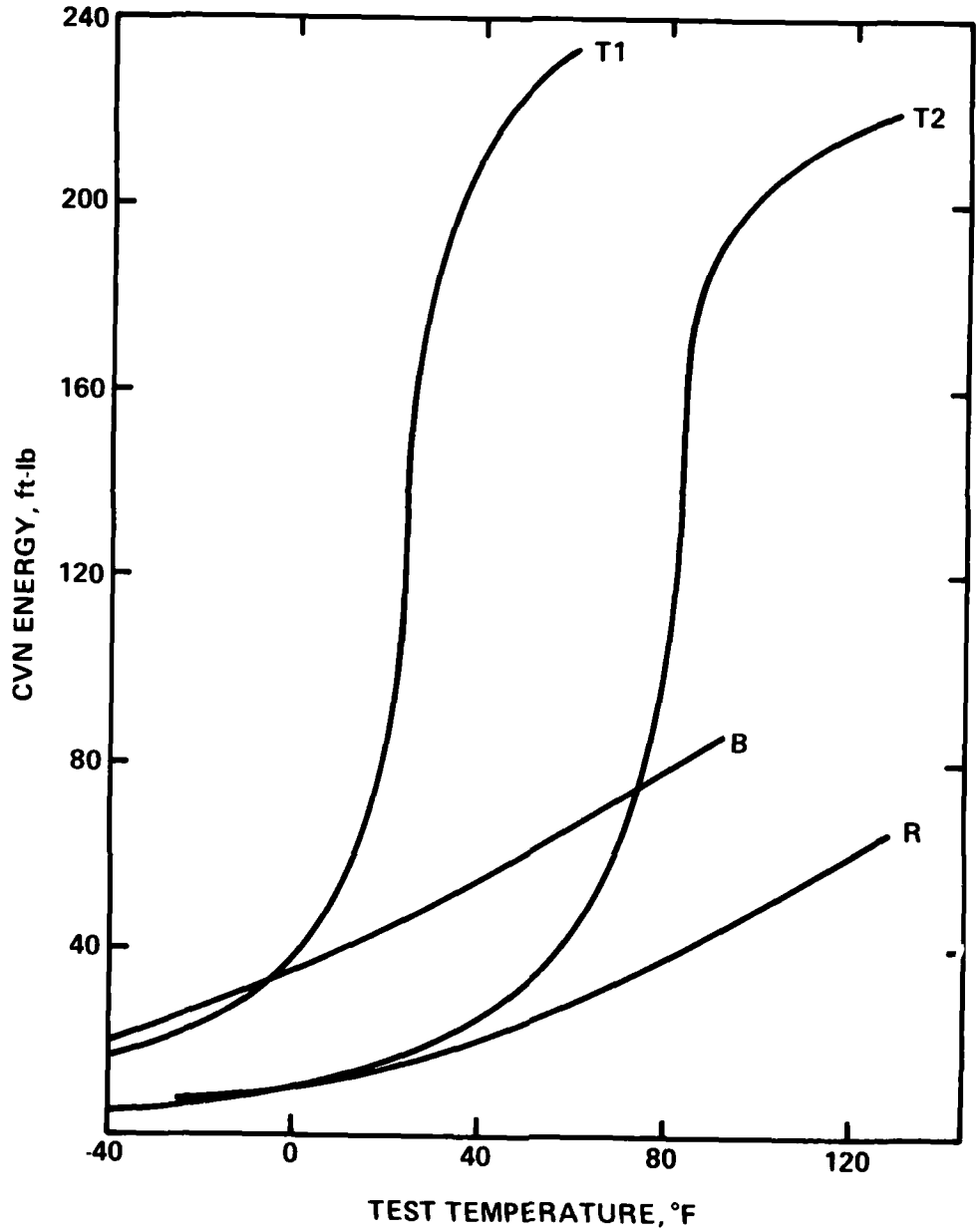

Figure 9. ESW-HAZ ENERGY-ABSORPTION TRANSITION CURVES TYPICAL OF Ti-BEARING STEELS (T1, T2) AND Ti-FREE STEELS (B, R)

STEEL T-1
TITANIUM STEEL

X150

STEEL T-2
TITANIUM-PLUS-HIGH-NITROGEN STEEL

X150

STEEL V-Ti-N
TITANIUM-PLUS-VANADIUM STEEL

X150

FRACTOGRAPHS OF CHARPY V-NOTCH SPECIMENS SHOWING CLEAVAGE FRACTURE IN THE GRAIN-COARSENED HAZ. (GLEEBLE SIMULATION OF ELECTROSLAG WELDING WITH 1000 kJ PER INCH HEAT INPUT) – PHASE III STEELS CONTAINING TITANIUM.

Figure 10

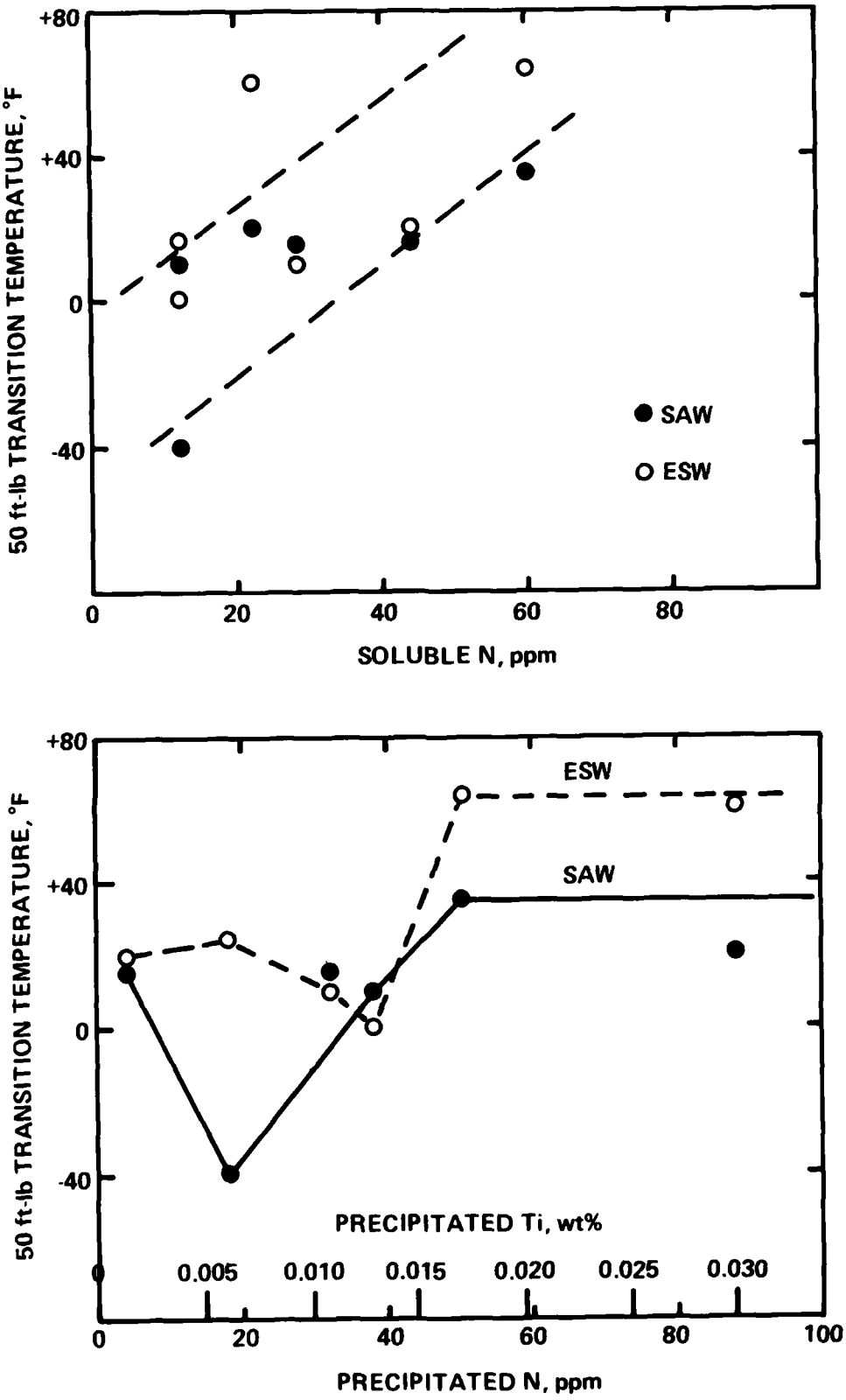

Figure 11. RELATION BETWEEN SOLUBLE AND PRECIPITATED NITROGEN AND THE HAZ-50-ft-lb TRANSITION TEMPERATURES

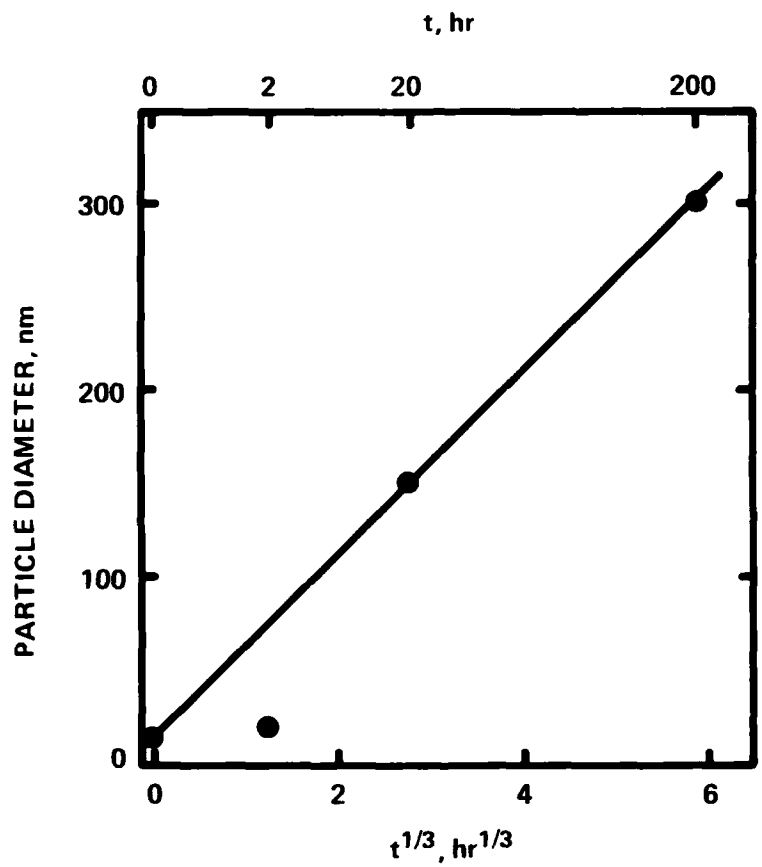

Figure 12. GROWTH OF TiN PARTICLES WITH TIME AT 2200°F. STEEL T3.

RL-2-8401

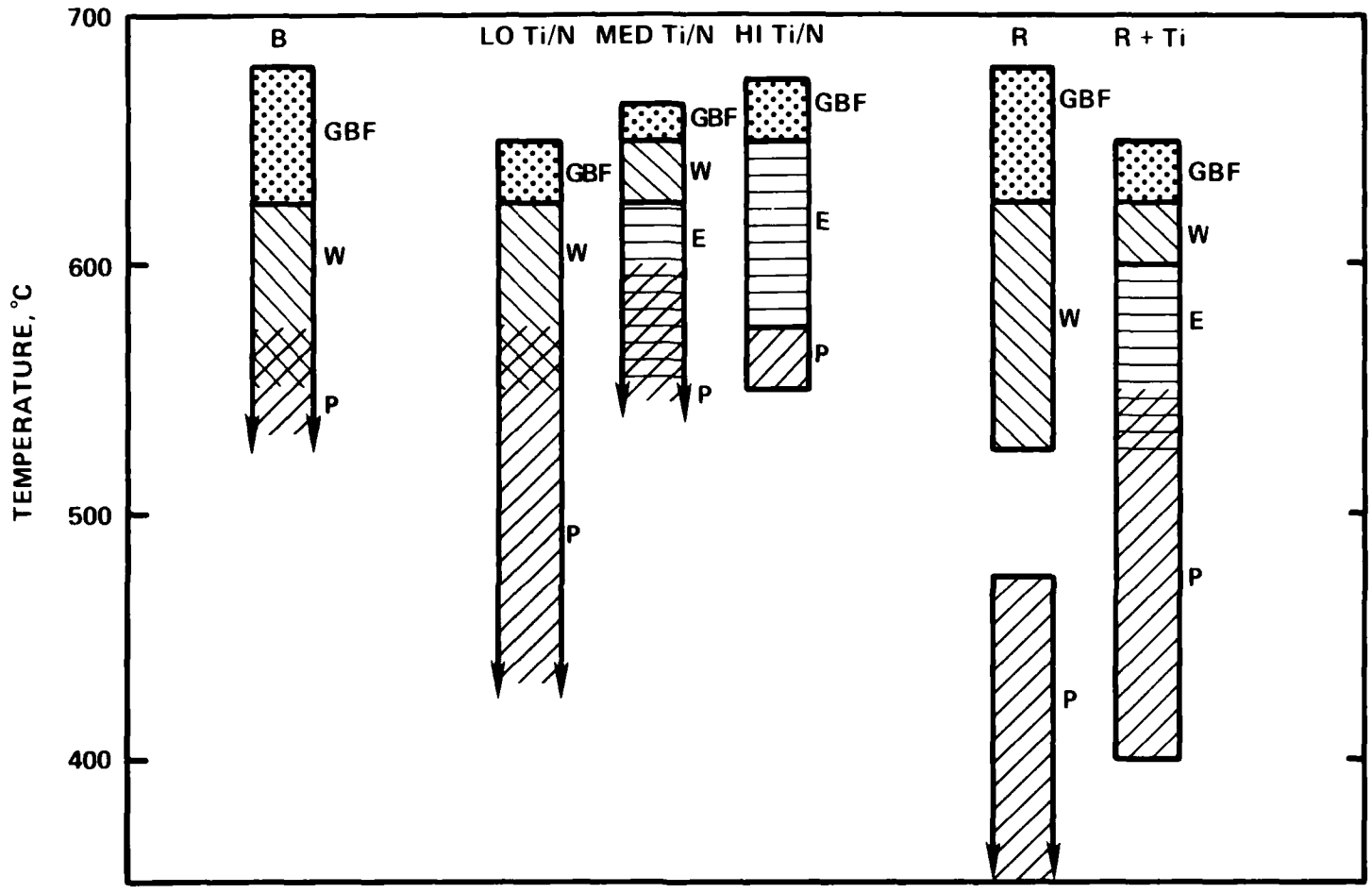

Figure 13. TEMPERATURE RANGES IN WHICH VARIOUS TRANSFORMATION PRODUCTS FORMED IN SIX STEELS DURING COOLING FROM THE ESW CYCLE (ARROWS INDICATE PEARLITE FORMATION IS INCOMPLETE). °F = 9/5°C + 32

GBF = GRAIN BOUNDARY FERRITE E = EQUIAXED FERRITE
W = WIDMANSTATTEN FERRITE P = PEARLITE

RL-2-8399

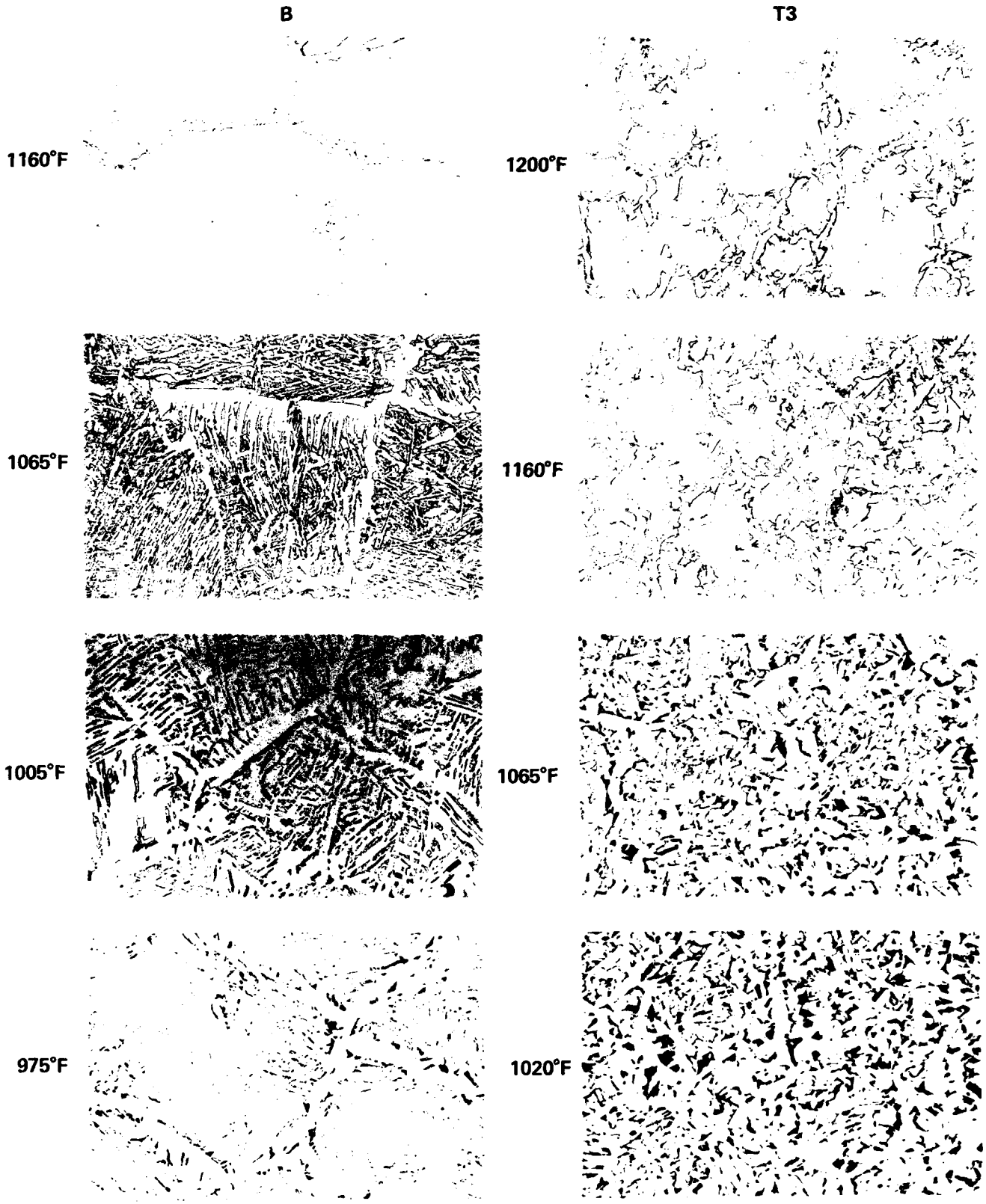

Figure 14. THE DEVELOPMENT OF TRANSFORMATION PRODUCTS IN THE HAZ OF THREE STEELS (B, T3, R) DURING COOLING IN THE ESW CYCLE. 100X.

R

1160°F

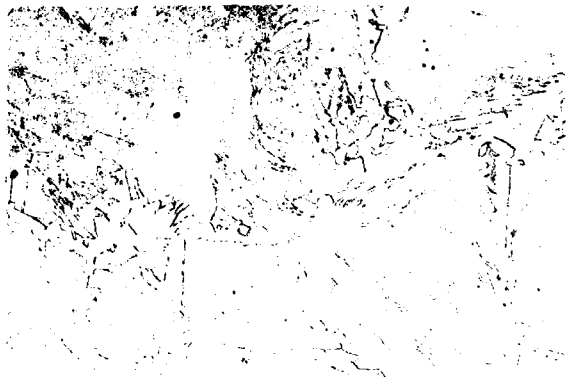

1005°F

795°F

660°F

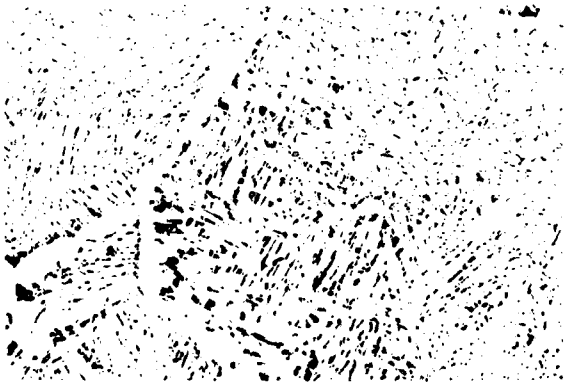

Figure 14. CONTINUED. 100X.

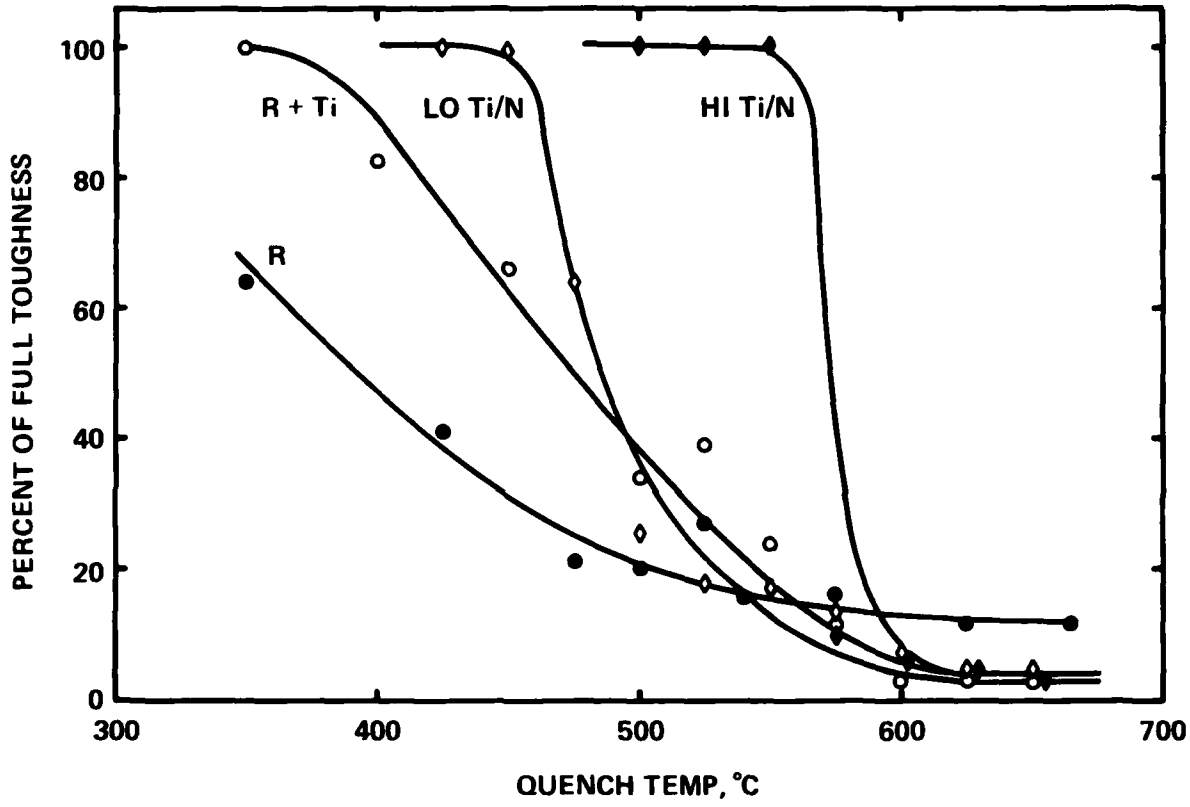

Figure 15. DEVELOPMENT OF TOUGHNESS DURING COOLING FROM AN ESW CYCLE. °F = 9/5°C + 32

RL-2-8400

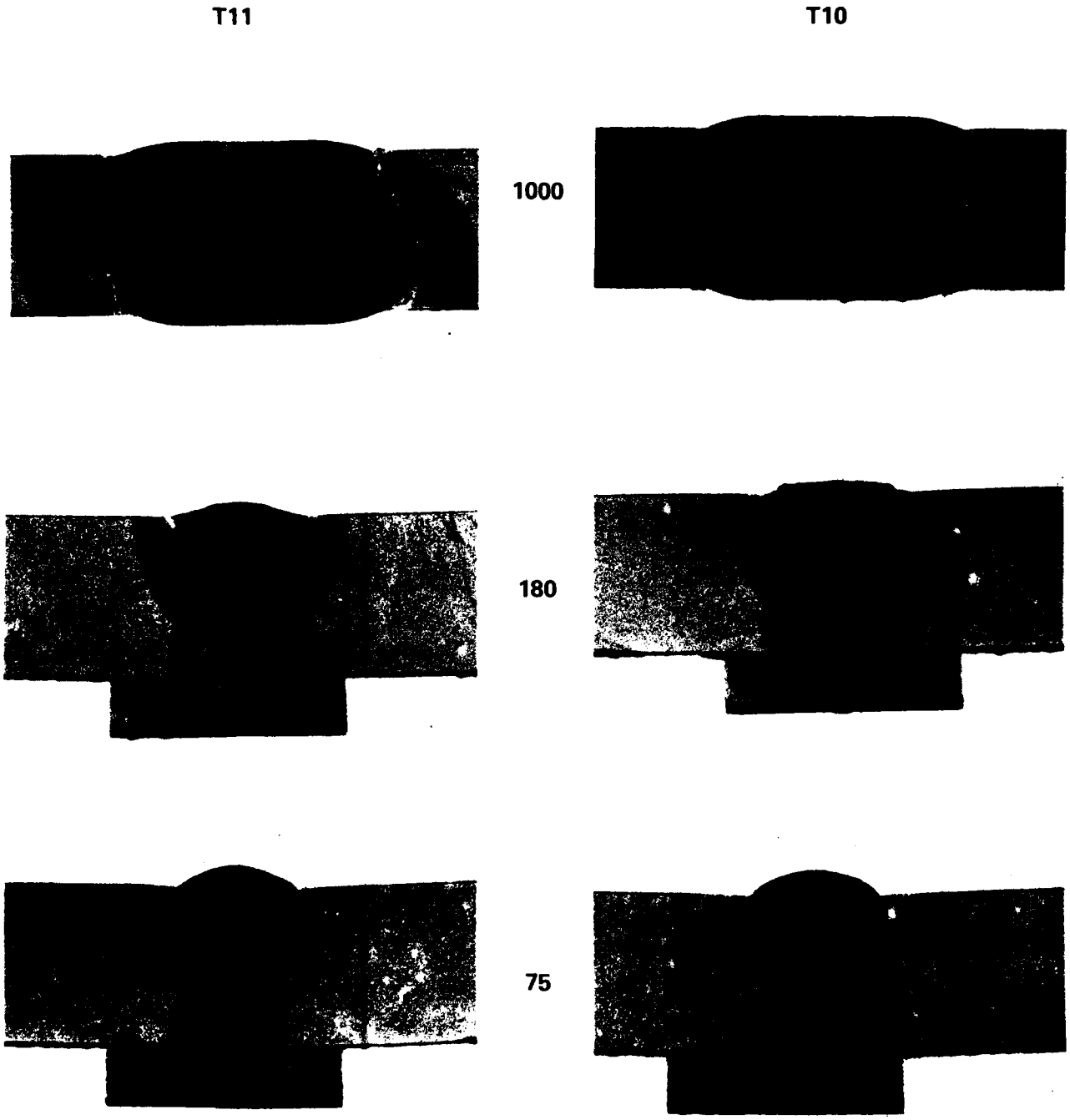

Figure 16. MACROGRAPHS OF WELDS IN STEELS T11 AND T10 AT THREE HEAT INPUTS; 1000 KJ/inch, 180 KJ/inch, and 75 KJ/inch

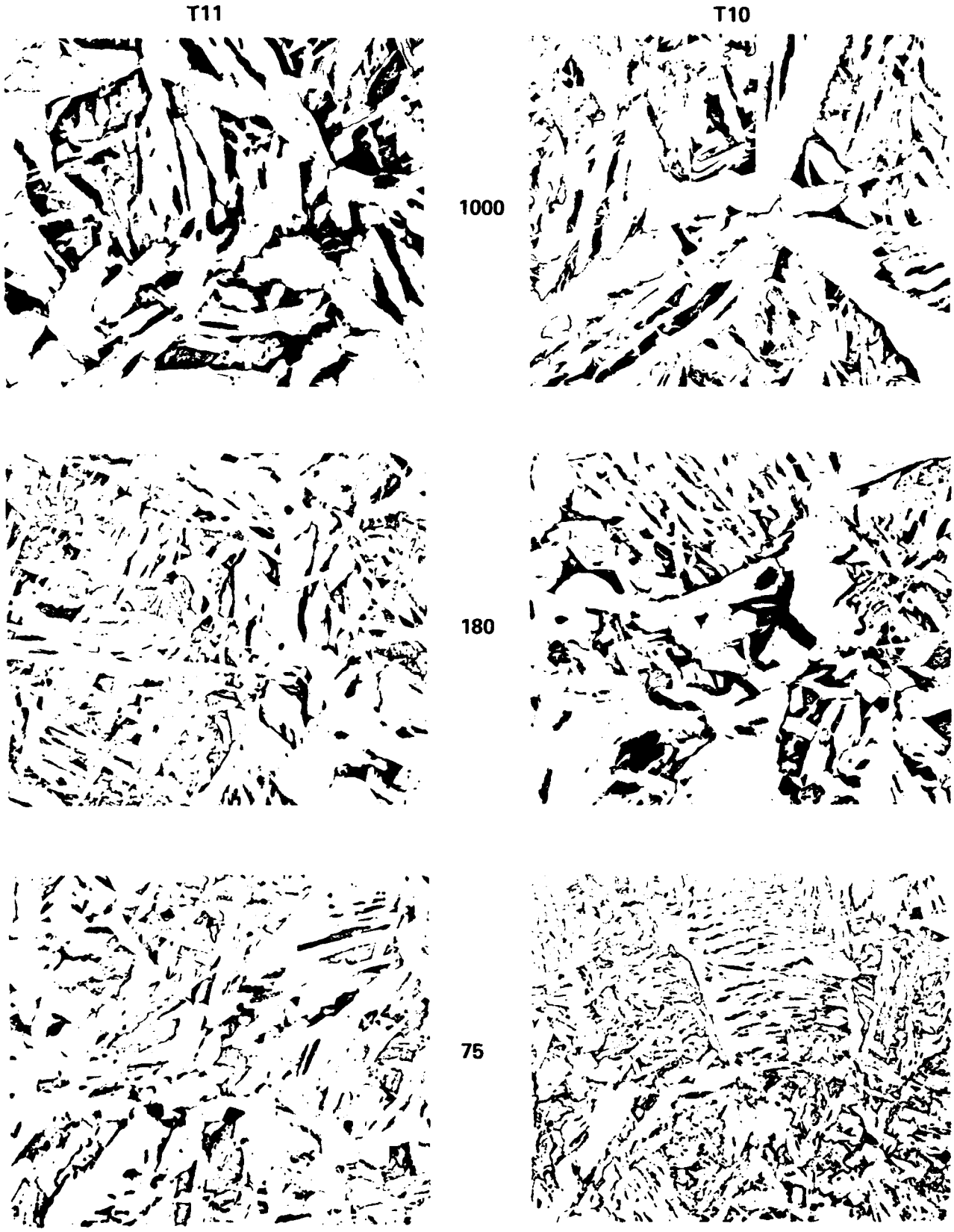

Figure 17. MICROSTRUCTURES IN THE HAZ OF WELDS OF STEELS T11 (LEFT) AND T10 (RIGHT) AT THREE HEAT INPUTS; 1000 KJ/inch ESW (TOP), 180 KJ/inch SAW (CENTER), AND 75 KJ/inch SAW (BOTTOM)

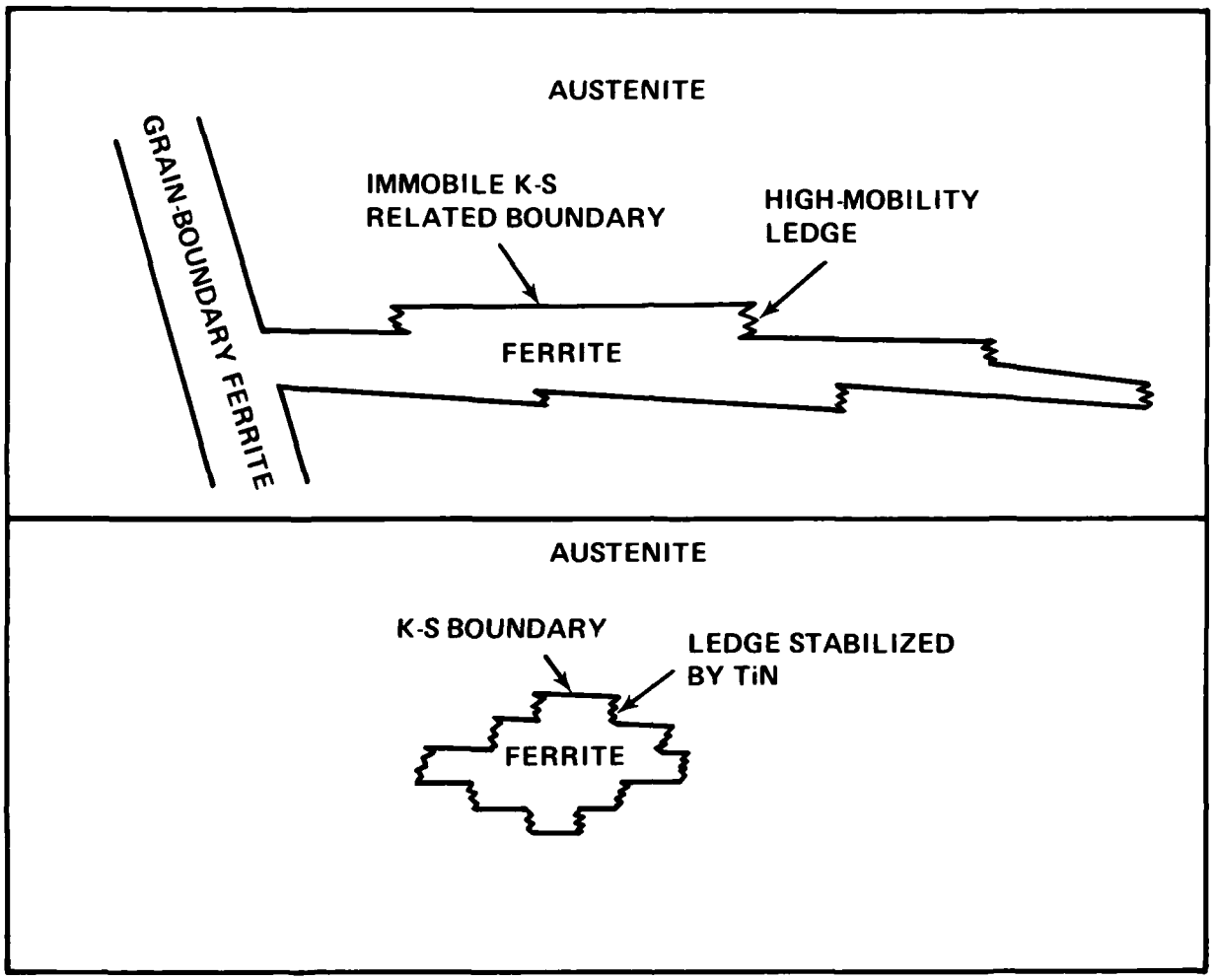

Figure 18 – GROWTH OF FERRITE: TOP- IN THE BASE STEEL BY UNRESTRICTED LEDGE MIGRATION; BOTTOM- IN A Ti-BEARING STEEL WHERE LEDGE MIGRATION IS INHIBITED BY TiN PARTICLES

Appendix A

Temperature Measurements at 1 mm From the Fusion Line in Weld Heat-Affected Zones of 1-Inch-Thick Plates

Electroslag Weld		180 kJ/in. Submerged-Arc Weld	
Time, sec	Temperature, °F	Time, sec	Temperature, °F
0	75	0	192
600	500	4	232
660	1000	9	2545
690	2100	13	2505
700	2525	17	2381
708	2522	22	2232
712	2484	26	2090
717	2443	31	1965
721	2402	35	1843
725	2322	39	1730
729	2278	43	1632
734	2227	48	1550
742	2148	52	1483
759	2042	56	1428
768	2003	60	1380
776	1922	69	1301
785	1843	77	1241
802	1716	86	1195
819	1602	94	1160
836	1502	103	1133
853	1414	112	1104
874	1320	125	1052
899	1231	134	1019
933	1133	146	973
971	1046	168	915
1024	950	180	884
1066	869	205	831
1125	773	222	801
1185	695	266	738
1245	627	387	624
1305	574	498	552
1365	527	618	498
1425	490	679	475

Appendix B

Individual Transverse Charpy V-Notch Test Results from Base Plates

Steel Code	Test Temperature, °F	Energy Absorbed, ft-lb	Shear Fracture, %	Lateral Expansion, mils
B	0	239	100	-
	-50	238	100	-
	-75	239	100	-
	-85	239	100	-
	-90	148	40	103
	-105	30	10	22
	-125	15	5	12
R	-100	171,237	55,100	105
	-105	239	100	-
	-125	151	40	108
	-150	12	5	10
T1	+40	239	100	-
	0	239	100	-
	-50	239	100	-
	-60	239	100	-
	-65	239	100	-
	-70	91	35	74
	-75	9,12	10,10	9,16
	-90	10	15	10
	-125	5	3	4
T7	+40	239	100	-
	-25	239	100	-
	-40	239	100	-
	-45	238	100	81
	-50	184,135	60,35	96,95
	-75	85,116	35,30	70,89
	-100	17	10	14
	-125	5	5	2
	-150	4	2	5
T5	-50	239	100	-
	-60	167	55	103
	-65	165	50	101
	-75	125,55	25,30	46,48
	-125	6	5	4
	-150	4	2	3
T4	-50	239	100	-
	-65	239	100	-
	-70	239	100	-
	-75	13,115,10	15,30,20	14,93,14

Appendix B (Continued)

Steel Code	Test Temperature, °F	Energy Absorbed, ft-lb	Shear Fracture, %	Lateral Expansion, mils
	-90	11	15	11
	-125	7	5	5
	-150	3	1	2
V1	-50	235	100	83
	-60	121	40	96
	-65	33,214,127	15,100,35	31,96,97
	-75	131,169	35,55	100,105
	-90	16	15	14
	-125	13	5	9
	-150	7	3	8
V2	0	195	80	96
	-25	213	100	93
	-50	148,114	50,40	97,84
	-75	95,146	35,50	76,105
	-125	8	5	6
	-150	8	3	4
T2	-50	239	100	-
	-60	239	100	-
	-65	135	45	43
	-75	121,150	40,40	90,105
	-100	20	10	16
	-125	6	5	6
	-150	4	2	4
T3	-25	239	100	-
	-35	239	100	-
	-45	118	35	93
	-50	120	35	90
	-60	116	35	94
	-75	15,35	15,20	13,51
	-100	7	5	16
	-125	5	3	4
	-150	3	1	7
T6	-50	239	100	-
	-55	118	35	95
	-60	133	40	105
	-75	11,13	15,15	17,12
	-125	5	3	4
	-150	3	0	6
VTN	-50	239	100	-
	-65	239	100	-
	-70	128	45	95

Appendix B (Continued)

Steel Code	Test Temperature, °F	Energy Absorbed, ft-lb	Shear Fracture, %	Lateral Expansion, mils
	-75	119,146	35,45	90,101
	-90	113	35	88
	-125	5	5	4
	-150	4	2	5
T10	0	240	100	-
	-40	240	100	-
	-60	240	100	-
	-80	138,118	100,30	103,67
	-100	14,130,118	5,50,45	14,95,97
	-120	8	0	5
T11	0	240	100	-
	-40	240	100	-
	-60	240	100	-
	-80	240	100	-
	-100	20,14	5,10	17,12
	-120	7	0	5
	-150	6	5	6
T8	0	219	78	-
	-20	108	83	30
	-40	119,219	91,92	40,-
	-60	103,85	85,70	25,25
	-80	68,105	59,90	15,25
	-100	95,73	85,66	30,15
	-120	45	39	5
	-150	20	17	0
T9	0	219	107	-
	-40	219	104	-
	-60	219,219	107,112	-
	-80	117,218	94,105	50,-
	-100	74,88	62,76	5,15
	-120	120,91	98,77	15,15
	-150	13	11	0
VT	0	145	98	65
	-40	219,111	102,77	-,60
	-60	118,127	95,98	50,50
	-80	119	97	50
	-100	109	90	15
	-120	42	35	5
	-150	32,6	25,3	1,0
	-180	8	11	0

Appendix C

Individual Charpy V-Notch Test Results of Specimens From the HAZ of ESW and SAW Gleeble Simulations

Steel Code	Test Temperature, °F	Energy Absorbed, ft-lb	Shear Fracture, %	Lateral Expansion, mils
		ESW Simulation		
B	+75	77	35	67
	+40	80,21	30,0	72,19
	0	90,11	30,15	86,20
	-40	33	0	26
R	+120	59	50	53
	+75	38	10	38
	+40	11	5	13
	0	18,7	10,0	16
	-40	7	0	8
T1	+40	218	98	99
	+20	123	40	87
	0	218,24	98,35	98
	-40	20,11	5,0	19,11
T7	+75	218	98	80
	+40	125	55	83
	0	75,28	35,30	62,29
	-40	55,17	30,15	49,20
T5	+75	140	65	82
	+40	131	55	88
	0	21,10	15,8	26,11
	-40	10,5	8,5	11,10
T4	+75	129	70	93
	+40	98,8	45,15	66,12
	0	88,72	35,35	68,58
	-40	12,8	2,15	11,12
V1	+75	68	30	56
	+40	49	30	42
	0	30	10	26
	-40	31,4	0,2	28,6
	-80	5	0	7
V2	+120	50	50	49
	+75	29	25	25
	+40	19	2	20
	0	11,9	0,8	10,10
	-40	6	0	7

Appendix C (Continued)

Steel Code	Test Temperature, °F	Energy Absorbed, ft-lb	Shear Fracture, %	Lateral Expansion, mils
T2	+120	218	98	110
	+75	127	70	86
	+40	17	25	18
	0	20,15	10,8	22,19
	-40	5	0	5
T3	+75	218	98	99
	+40	28	15	28
	0	12,10	20,10	17,9
	-40	7	5	8
T6	+75	219	98	96
	+60	218	98	96
	+40	26	25	30
	0	23,15	20,20	26,17
	-40	5	2	6
VTN	+120	98	40	88
	+75	98,10	40,15	73,12
	+40	22	15	20
	0	5	0	3
	-40	4	0	3
T8	+40	99,71	50,45	71,59
	0	40,15	18,20	35,19
	-20	20,12	10,15	18,14
	-40	17,16	25,20	17,14
T9	+70	99,55	50,45	50,55
	+40	50,31	20,15	25,42
	+20	31,24	8,8	27,22
	0	12,12	8,5	13,11
VT	+120	63,47	35,40	55,44
	+75	35,31	35,30	32,29
	+40	22,14	15,15	20,15
	0	19,11	5,5	15,10
T10	+40	117,53	40,25	79,46
	0	133,28,22	45,20,15	83,26,22
	-20	47	20	37
	-40	12,8	10,15	14,05
T11	+40	144,36	50,25	88,28
	0	93,76,32	35,30,20	70,57,27
	-20	22	20	20
	-40	53,10	10,10	44,09

Appendix C (Continued)

Steel Code	Test Temperature, °F	Energy Absorbed, ft-lb	Shear Fracture, %	Lateral Expansion, mils
		SAW Simulation		
B	+75	108	83	67
	+40	129,11,115	90,14,92	75,5,65
	0	14,23	14,23	2,0
	-40	10	9	2
R	+75	58	49	25
	+40	22	24	15
	0	11	10	2
	-40	19,12	15,11	1,0
T1	+40	176	80	80
	0	120,11,116	86,16,87	55,15,40
	-40	14,9	14,9	15,15
T7	+40	110	75	55
	0	105,18,100	77,22,75	40,20,30
	-40	13,15	15,18	25,15
T5	+40	51,121	43,79	25,55
	0	25,66	25,56	15,20
	-40	9,10	10,10	8,2
T4	+75	49	42	25
	+40	22,68	26,53	30,25
	0	37,10	31,11	8,8
	-40	7	7	7
V1	+75	91	88	35
	+40	27,64	24,52	20,15
	0	27,17	23,16	5,0
	-40	12	10	0
V2	+75	42	37	35
	+40	14,20	17,23	15,10
	0	15,19	14,20	10,5
	-40	9	7	7
T2	+75	98,111	67,76	55,70
	+40	88	78	45
	0	12,66,13	14,56,16	25,35,8
	-40	8,6	8,5	15,8
T3	+75	37	39	25
	+40	120	80	55
	0	42,18	37,18	25,18
	-40	8,8	9,10	20,12

Appendix C (Continued)

Steel Code	Test Temperature, °F	Energy Absorbed, ft-lb	Shear Fracture, %	Lateral Expansion, mils
T6	+75	56	48	45
	+40	37	33	25
	0	9,77	10,63	15,35
	-40	9,8	12,16	8,5
VTN	+75	69,30	54,29	35,35
	+40	19,67	21,52	22,18
	0	6,7	9,7	5,2
	-40	5	5	0
T8	+75	103	77	75
	+40	63	54	45
	0	42,56	35,46	8,20
	-40	37,41	30,32	15,15
	-80	14,11	9,9	0,0
T9	+75	94	72	50
	+40	11,50	12,44	15,25
	0	15,45,18	15,37,19	15,18,8
	-40	8	8	1
VT	+75	70	56	45
	+40	18,30	16,29	10,12
	0	17,47,11	17,37,11	8,15,6
	-40	7	6	1
T10	+40	115	45	79
	0	67,92	20,35	50,72
	-40	50,70	15,20	38,48
	-80	29,12	5,5	18,6
	-100	3	0	1
T11	+40	122,74	45,30	79,58
	0	9,74,48	15,20,20	10,56,40
	-20	22	10	17
	-40	6,12	10,10	4,6

Appendix D

Individual Charpy V-Notch Test Results from the HAZ of Electroslag and Submerged-Arc Welded Steel Plates

Steel Code	Test Temperature, °F	Distance from Fusion Line, mm	Energy Absorbed, ft-lb	Shear Fracture, %	Lateral Expansion, mils
			Electroslag Welded (~1000 kJ/inch)		
T10	0	0	69,77,73,43	25,20,20,15	57,64,60,39
		1	25,48,142,112	25,20,60,45	26,40,96,86
		3	115,124,117,100	35,35,35,30	87,90,87,82
	-40	0	12,10,24,11	5,5,10,5	9,9,18,8
		1	42,18,38,42	20,15,15,15	28,14,26,31
		3	57,63,118,22	20,20,45,15	43,43,94,18
T11	0	0	16,13,57,13	15,15,20,10	16,12,44,15
		1	28,25,35,128	30,30,20,45	28,24,41,92
		3	115,113,119,118	45,40,45,45	91,89,89,90
	-40	0	18,14,20,17	20,5,10,10	15,10,14,08
		1	11,10,13,13	5,5,5,5	04,06,13,16
		3	97,33,18,106	35,15,15,35	75,30,18,86
			Two-Pass Submerged-Arc Welded (~180 kJ/inch)		
T10	0	0	52,36,48,37	35,40,35,30	45,28,36,29
		1	120,115,127,124	45,45,45,50	83,87,85,91
		3	196,186,202,161	100,100,100,100	88,87,93,97
	-40	0	18,46,53,36	20,25,25,20	13,31,38,26
		1	102,35,49,48	45,20,25,25	78,27,41,37
		3	100,159,129,128	45,55,55,50	73,90,91,87
T11	0	0	25,35,100,128	45,40,45,40	25,30,71,98
		1	40,120,123,33	40,45,50,35	33,79,93,25
		3	146,142,156,167	70,60,100,100	86,85,82,89

Appendix D (Continued)

Steel Code	Test Temperature, °F	Distance from Fusion Line, mm	Energy Absorbed, ft-lb	Shear Fracture, %	Lateral Expansion, mils
	-40	0	14,28,08,40	25,30,20,20	15,29,9,34
		1	15,39,30,12	20,25,20,15	15,31,24,11
		3	143,139,150,168	55,45,95,90	89,98,101,103
		Six-Pass Submerged-Arc Welded (~75 kJ/inch)			
T10	0	0	148,161,171,174	80,100,100,100	97,91,97,99
		1	184,210,194,172	100,100,100,100	97,98,90,78
		3	193,152,149,188	100,80,75,100	88,83,89,90
	-40	0	112,178,128,178	45,100,60,100	79,98,89,99
		1	181,156,136,134	100,100,80,50	95,99,78,86
		3	138,140,137,138	60,55,55,60	90,86,94,94
T11	0	0	141,141,159,158	55,70,100,100	86,85,92,87
		1	161,148,173,181	100,100,100,100	101,97,100,99
		3	157,159,151,205	100,100,100,100	90,90,94,84
	-40	0	127,119,131,45	60,40,95,70	78,119,131,45
		1	112,34,184,63	45,30,100,100	83,27,90,90
		3	127,150,137,137	45,100,50,45	98,99,82,91

☆ U.S. GOVERNMENT PRINTING OFFICE : 1985 O - 486-335

COMMITTEE ON MARINE STRUCTURES
Commission on Engineering and Technical Systems
National Academy of Sciences - National Research Council

The COMMITTEE ON MARINE STRUCTURES has technical cognizance of the interagency Ship Structure Committee's research program.

Mr. A. Dudley Haff, Chairman, Annapolis,MD
Prof. Alfredo H.-S. Ang, University of Illinois, Urbana, IL
Mr. Griff C. Lee, Griff C. Lee, Inc., New Orleans, LA
Mr. Peter W. Marshall, Shell Oil Company, Houston, TX
Mrs. Margaret D. Ochi, Gainesvuille, FL
Prof. David L. Olson, Colorado School of Mines, Goldon, CO
Mr. Richard W. Rumke, Executive Secretary, Committee on Marine Structures

The LOADS ADVISORY GROUP

Mr. Peter W. Marshall, Chairman, Shell Oil Company, Houston, TX
Prof. Robert F. Beck, University of Michigan, Ann Arbor, MI
Prof Colin B. Brown, University of Washington, Seattle, WA
Mr. John C. Estes, Zapata Offshore Company, Houston, TX
Mr. Joseph P. Fischer, American Steamship Company, Buffalo, NY
Prof. Joseph P. Murtha, University of Illinois, Urbana, IL
Mr. Robert J. vom Saal, Bethlehem Steel Corporation, Sparrows Point, MD
Prof. Paul H. Wirsching, University of Arizona, Tucson, AZ

The MATERIALS ADVISORY GROUP

Prof. David L. Olson, Chairman, Colorado School of Mines
Mrs. Nancy C. Cole, Combustion Engineering, Inc., Chatanooga, TN
Prof. George T. Hahn, Vanderbilt University, Nashville, TN
Prof. William T. Hartt, Florida Atlantic University, Boca Raton, FL
Dr. Santiago Ibarra, Gulf Science and Technology Company, Pittsburgh, PA
Mr. John J. Schmidt, Lukens, Inc., Coatesville, PA
Mr. Robert E. Sommers, Welding Consultant, Hellertown, PA
Dr. Nicholas Zettlemoyer, Exxon Production Research Company, Houston, TX

SHIP STRUCTURE COMMITTEE PUBLICATIONS

SSC-317	Determinsation of Strain Rates in Ship Hull Structures: A Feasibility Study by J. G. Giannotti and K. A. Stambaugh, 1984
SSC-319	Development of A Plan to Obtain In-Service Still-Water Bending Moment Information for Statistical Characterization by J. W. Boylston and K. A. Stambaugh, 1984
SSC-321	Survey of Experience Using Reinforced Concrete in Floating Marine Structures by O.H. Burnside and D.J. Pomerening, 1984
SSC-322	Analysis and Assessment of Major Uncertainties Associated With Ship Hull Ultimate Failure by P. Kaplan, M. Benatar, J. Bentson and T.A. Achtarides, 1984
SSC-323	Updating of Fillet Weld Strength Parameters for Commercial Shipbuilding by R.P. Krumpen, Jr., and C.R. Jordan, 1984
SSC-324	Analytical Techniques for Predicting Grounded Ship Response by J.D. Porricelli and J.H. Boyd, 1984
SSC-325	Correlation of Theoretical and Measured Hydrodynamic Pressures for the SL-7 Containership and the Great Lakes Bulk Carrier S. J. Cort by H.H. Chen, Y.S. Shin & I.S. Aulakh, 1984
SSC-326	Long-Term Corrosion Fatigue of Welded Marine Steels by O.H. Burnside, S.J. Hudak, E. Oelkers, K. Chan, and R.J. Dexter, 1984
SSC-327	Investigation of Steels for Improved Weldability in Ship Construction by L.J. Cuddy, J.S. Lally and L.F. Porter 1985
SSC-328	Fracture Control for Fixed Offshore Structures by P.M. Besuner, K. Ortiz, J.M. Thomas and S.D. Adams 1985
SSC-329	Ice Loads and Ship Response to Ice by J.W. St. John, C. Daley, and H. Blount, 1985
SSC-330	Practical Guide for Shipboard Vibration Control by E.F. Noonan G.P. Antonides and W.A. Wood, 1985
None	Ship Structure Committee Publications - A Special Bibliography, AD-A140339

END

FILMED

1-86

DTIC